Fluid migration pathways to seafloor seepage in inner Isfjorden and Adventfjorden, Svalbard

Srikumar Roy, Kim Senger, Alvar Braathen, Riko Noormets, Martin Hovland & Snorre Olaussen

Roy, S., Senger, K., Braathen, A., Noormets, R., Hovland, M. & Olaussen, S.: Fluid migration pathways to seafloor seepage in inner Isfjorden and Adventfjorden, Svalbard. *Norwegian Journal of Geology,* Vol 94, pp. 99–119. Trondheim 2014, ISSN 029-196X.

This study represents a marine baseline study for the Longyearbyen CO_2 Lab, in which CO_2 may be injected in the Upper Triassic–Middle Jurassic Kapp Toscana Group, which comprises several permeable beds. The target saline aquifer dips 1–3° southwest and thus crops out 14–16 km northeast from the proposed injection site in both offshore and onshore settings. Since the aquifer is exposed at the surface, a carefully documented pre-injection baseline study is required prior to any injection. The seafloor and its subsurface conditions are analysed and interpreted, where the targeted aquifer and organic-rich top-seal shales sub-crop. High-resolution multibeam bathymetric and backscatter imaging, sub-bottom acoustic profiles, sidescan sonar data and multichannel 2D seismic data were used to analyse seepage-related features on the seafloor and their link to subsurface tectonic structures. In total, 398 pockmarks have been identified on the seafloor, suggesting significant past and/or present natural fluid seepage. Beneath the pockmarks, acoustic features such as enhanced reflections, acoustic turbid zones and acoustic blankings interpreted on sub-bottom acoustic profiles suggest possible gas accumulation and migration linked to various fault systems reaching the seafloor. This paper discusses fluid migration in a fold-and-thrust belt setting, broadened by secondary sealing mechanisms in Arctic conditions. We conclude by illustrating the various types of reported fluid seepage, particularly along permeable fault planes and at the rims of igneous intrusions.

Srikumar Roy, Department of Arctic Geology, The University Centre in Svalbard, P.O. Box 156, 9171 Longyearbyen, Norway. Department of Earth Science, University of Bergen, Allégaten 41, 5007 Bergen, Norway. Present address: Schlumberger Norway Technology Center, P.O. Box 8013, 4068 Stavanger, Norway. Kim Senger, Department of Arctic Geology, The University Centre in Svalbard, P.O. Box 156, 9171 Longyearbyen, Norway. Department of Earth Science, University of Bergen, Allégaten 41, 5007 Bergen, Norway. Centre for Integrated Petroleum Research, Uni Research, Allégaten 41, 5007 Bergen, Norway. Alvar Braathen, Department of Arctic Geology, The University Centre in Svalbard, P.O. Box 156, 9171 Longyearbyen, Norway. Present address: Department of Geosciences, University of Oslo, Blindern, 0316 Oslo, Norway. Riko Noormets, Department of Arctic Geology, The University Centre in Svalbard, P.O. Box 156, 9171 Longyearbyen, Norway. Martin Hovland, Tech Team Solutions, Stavanger–4000, Norway. Snorre Olaussen, Department of Arctic Geology, The University Centre in Svalbard, P.O. Box 156, 9171 Longyearbyen, Norway.

E-mail corresponding author (Srikumar Roy): srikumar.roy@unis.no, srikumar.iitkgp@gmail.com

Published December 24. 2014.

Introduction

The injection and safe storage of anthropogenic CO_2 in deep geological reservoirs is a feasible strategy practised to reduce greenhouse CO_2 gas concentrations in the atmosphere (Lewicki et al., 2007; Bachu, 2008; Chadwick et al., 2009; Hosa et al., 2011). CO_2 has been injected into confined saline aquifers and depleted oil and gas reservoirs for decades to enhance recovery, providing safe storage of CO_2 in deep geological formations (Chadwick et al., 2009; Jenkins et al., 2012). The objective of the Longyearbyen CO_2 Lab project in Svalbard is to evaluate local geological conditions for subsurface storage of modest amounts of CO_2 in the target aquifer, comprising Upper Triassic–Middle Jurassic (Kapp Toscana Group) siliciclastics (Braathen et al., 2012). The target aquifer offers moderate secondary porosity (5–18%) and low permeability (1–2 mD) (Braathen et al., 2012; Ogata et al., 2012; Mørk, 2013). Water injection tests suggest good injectivity and lateral fluid flow in the layered aquifer succession, facilitated to a large degree by an extensive fracture network (Braathen et al., 2012; Ogata et al., 2012). A detailed study of the fracture sets, disaggregation deformation bands and their characteristics is discussed in light of the impact of the lithostructural domains on the fluid-flow pathways in the aquifer unit (Ogata et al., 2014). The Janusfjellet Subgroup forms the overlying top-seal of 250 m of paper shale (Middle–Upper Jurassic Agardhfjellet Formation) followed by 200 m of a shaly-silty lithology (Lower Cretaceous Rurikfjellet Formation). The entire aquifer and cap-rock succession dips on average 1–3° southwest and crops out 14–20 km northeast of the future injection site, in both onshore and offshore settings.

An understanding of the pre-injection geological setting and mapping of associated natural seeps in the vicinity of

the storage site is a pre-requisite to geological storage of CO_2. Such mapping targets onshore pingos (Yoshikawa & Harada, 1995; Ross et al., 2005) and seafloor pockmarks related to expulsion of fluids from shallow and deep sources in Spitsbergen (Roy et al., 2012). This study documents the distribution of pockmarks and discusses their likely formation mechanisms linked to potential fluid migration pathways. The findings of this integrated geophysical analysis will form the baseline for future monitoring of the Longyearbyen CO_2 Lab project. In particular, this study addresses: (i) the extent of the targeted Kapp Toscana Group (top) aquifer in the offshore setting, (ii) the distribution of pockmarks on the seafloor covered by the Kapp Toscana Group in inner Isfjorden and the Adventdalen Group in Adventfjorden, (iii) the shallow gas occurrences within the Late Weichselian–Holocene marine sediments, and (iv) the importance of thrust zones, steep small faults and other deep-rooted faults as potential fluid migration pathways.

Regional setting

The study area is situated on the northwestern margin of the major gentle syncline known as the Central Spitsbergen Basin of Svalbard (Steel et al., 1981), offering Palaeogene units in the centre and successively older units out from the syncline to the east, north and west, as shown in Figs. 1 & 2. The Svalbard archipelago represents an uplifted part of the northwest margin of the Barents shelf (Nøttvedt et al., 1993; Harland, 1997; Dallmann et al., 2002; Worsley, 2008), and is briefly summarised here. Five major stages in the geological evolution of Svalbard have been reviewed by Steel & Worsley (1984), Bergh et al. (1997) and Braathen et al. (2012). The basement comprises Precambrian to Early Palaeozoic metamorphic rocks (Hecla Hoek) unconformably overlain by Devonian and Carboniferous units in fault-bound basins (Steel & Worsley, 1984). The overlying units of the Upper Carboniferous and Lower Permian carbonates and evaporites were deposited as part of a stable platform succession. In the Triassic to Cretaceous, there was a shift to mainly siliciclastic deposits linked to stable platform conditions ranging from deep- to shallow-marine settings (Harland, 1997). Intrusions of predominantly doleritic rocks took place in Svalbard during Early Cretaceous at c. 124.5–122.2 Ma (Corfu et al., 2013), and these are well exposed in the present study area both onshore and offshore (Senger et al., 2013). This event coincides with a regional regression and deposition of fluvial sandstones followed by a gradual transgression, which is reflected in a transition to shallow-marine and deltaic deposits (Helvetiafjellet and Carolinefjellet formations). In the latest Cretaceous, a transform plate boundary developed between Greenland and the western Barents Sea (Talwani & Eldholm, 1977; Gaina et al., 2009). This caused Paleocene–Eocene transpressional shortening in a fold-thrust belt followed by Oligocene transtensional opening of the

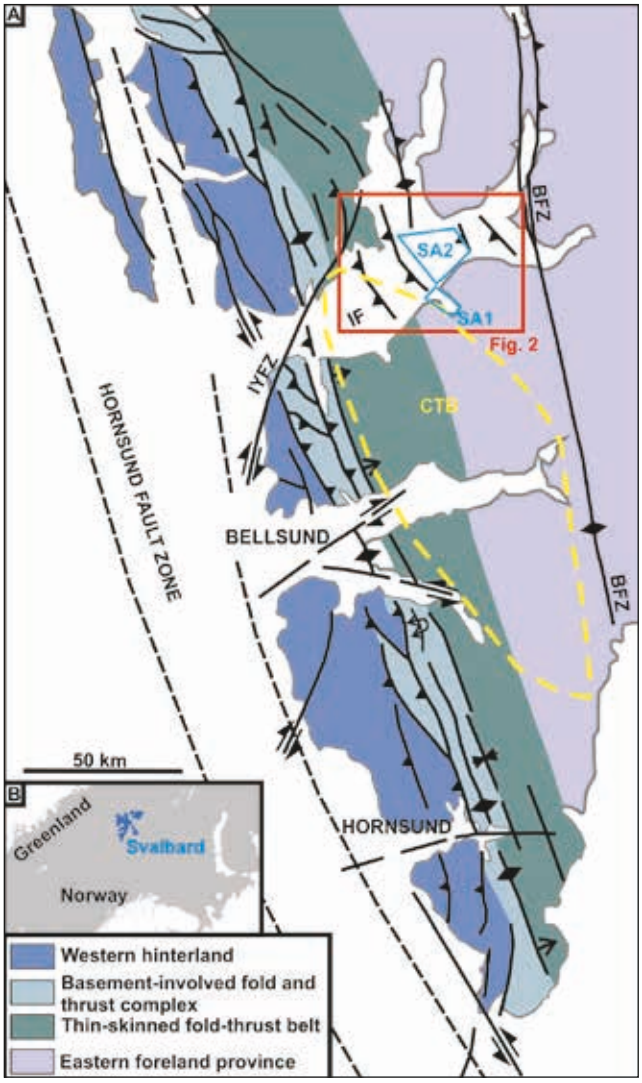

Figure 1. (A) Geotectonic map of south-central Svalbard based on Braathen et al. (2012) with the location of the study area shown in Central Isfjorden. (B) Location of Svalbard with respect to Norway and Greenland. Abbreviations: SA1: Study Area 1, SA2: Study Area 2 BFZ – Billefjorden Fault Zone, CTB – Central Tertiary Basin, IF – Isfjorden, IYFZ – Isfjorden–Ymerbukta Fault Zone.

northernmost Atlantic ocean basin (Braathen & Bergh, 1995; Bergh et al., 1997; Braathen et al., 1999; Leever et al., 2011). Contemporaneous sedimentary units of the Central Spitsbergen Basin are of Palaeogene age, deposited as a response to flexural subsidence of a foreland basin system during formation of the West Spitsbergen Fold-and-Thrust Belt (WSFTB) (Braathen et al., 1999). The WSFTB is characterised by a western thick-skinned province, or major basement-cored fold complex, and a thin-skinned fold-thrust belt with three distinct detachment levels to the east (Bergh et al., 1997; Braathen et al., 1999; Blinova et al., 2013). The sub-cropping bedrock in Isfjorden is blanketed by 10–50 m of Late Weichselian–Late Holocene glacial and post-glacial marine sediments (Forwick & Vorren, 2010).

The Upper Palaeozoic to Cenozoic stratigraphy of Svalbard is similar to that in the Barents Shelf area, the

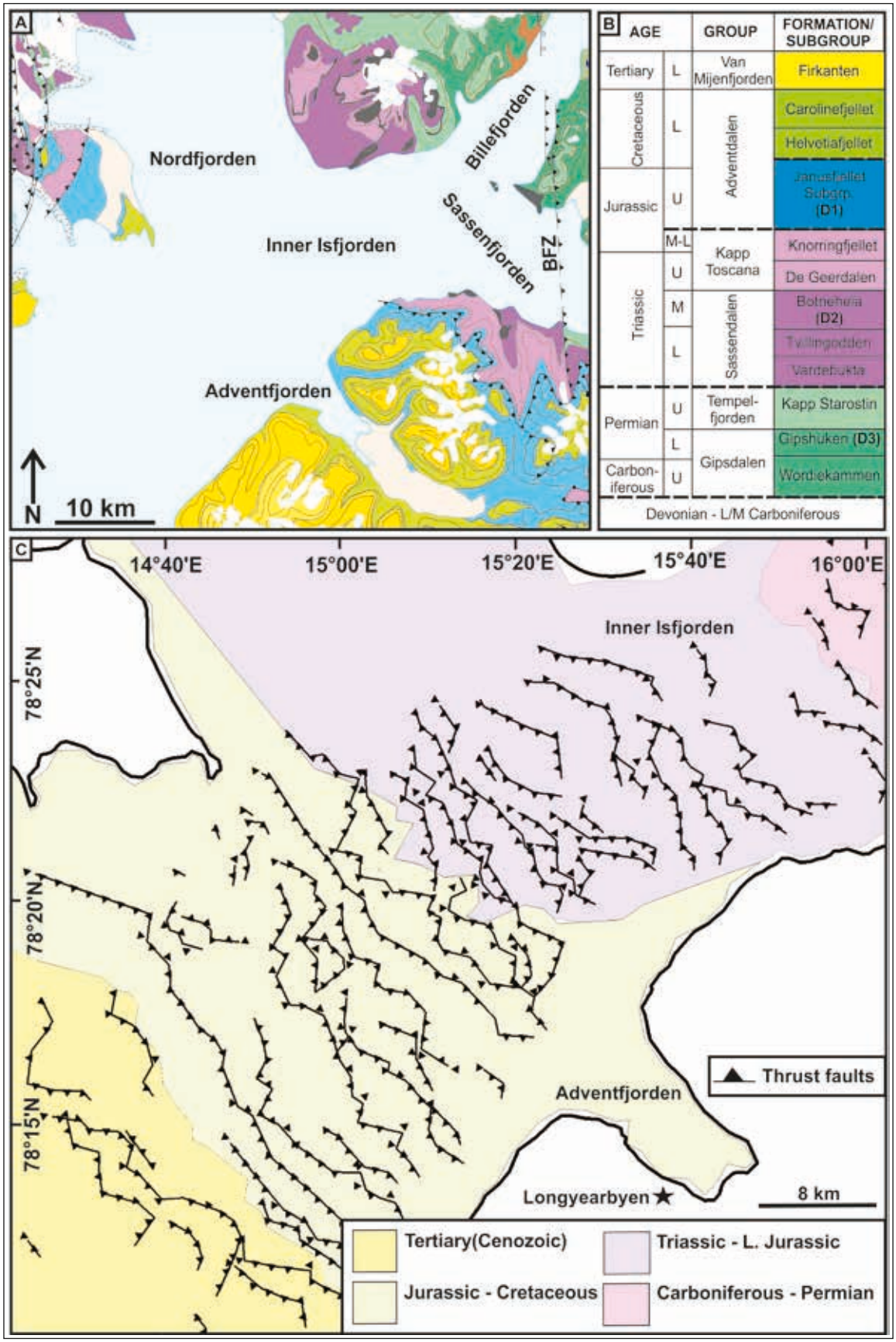

Figure 2. *(A) Terrestrial bedrock map of inner Isfjorden area (Dallmann et al., 2002). (B) Stratigraphic table of Spitsbergen (Bergh et al., 1997; Dallmann et al., 2002). The dashed lines indicate the geological unconformities which could be interpreted on the marine 2D seismic dataset. D1, D2 and D3 are décollement layers interpreted on the seismic dataset. (C) Submarine bedrock map and distribution of thrust faults in the inner Isfjorden area (Blinova et al., 2012; Roy et al., 2014).*

latter comprising several economic petroleum discoveries (Nøttvedt et al., 1993; Henriksen et al., 2011; Larssen et al., 2012). No commercial hydrocarbon discoveries were made on Spitsbergen despite drilling of 17 deep well. Although there have been numerous technical discoveries including over-pressured reservoirs along the southwest coast of Isfjorden and in the Billefjorden Trough, attesting to an active fluid migration system due to the presence of potential source rocks in Spitsbergen (Nøttvedt et al., 1993; Bjorøy et al., 2010). Evidence of past oil and gas seeps has been found in outcrops (Hammer et al., 2011) and in offshore sediments (Knies et al., 2004). Methane flux has been detected in the water column of western Spitsbergen (Damm et al., 2005). Pockmarks related to fluid expulsion have been identified on the seafloor of the greater Isfjorden fjord system (Forwick et al., 2009; Roy et al., 2012). This paper presents an analysis of fluid migration pathways from the underlying bedrock in the pockmarked areas of Central Isfjorden.

The studied region is subdivided into study areas 1 and 2 (SA1 and SA2) (Fig. 1). SA1 (Adventfjorden) comprises the offshore geological setting in the close vicinity of Longyearbyen and the planned injection site. The seafloor outcrop of SA1 consists of the cap-rock succession (Jurassic–Cretaceous rocks). On the contrary, SA2 includes the seafloor outcrop of both the cap rock and aquifer (Triassic–Cretaceous rocks). Accordingly, two fluid migration systems can be expected, which in concert allow insight into fluid-flow pathways within the targeted aquifer and the overlying cap-rock system.

Methods

High-resolution geophysical data

The following three different types of high-resolution geophysical data were collected in the two study areas (SA1 and SA2) (Fig. 3).

Multibeam bathymetric and backscatter data

The high-resolution multibeam bathymetric data were collected with a 95 kHz Kongsberg EM1002 multibeam echo sounder by the Norwegian Hydrographic Service in 2008. The processed data were gridded with a 5 m horizontal cell size using IVS Fledermaus 7.0 software for visual examination of the morphology of the pockmarks and other submarine landforms.

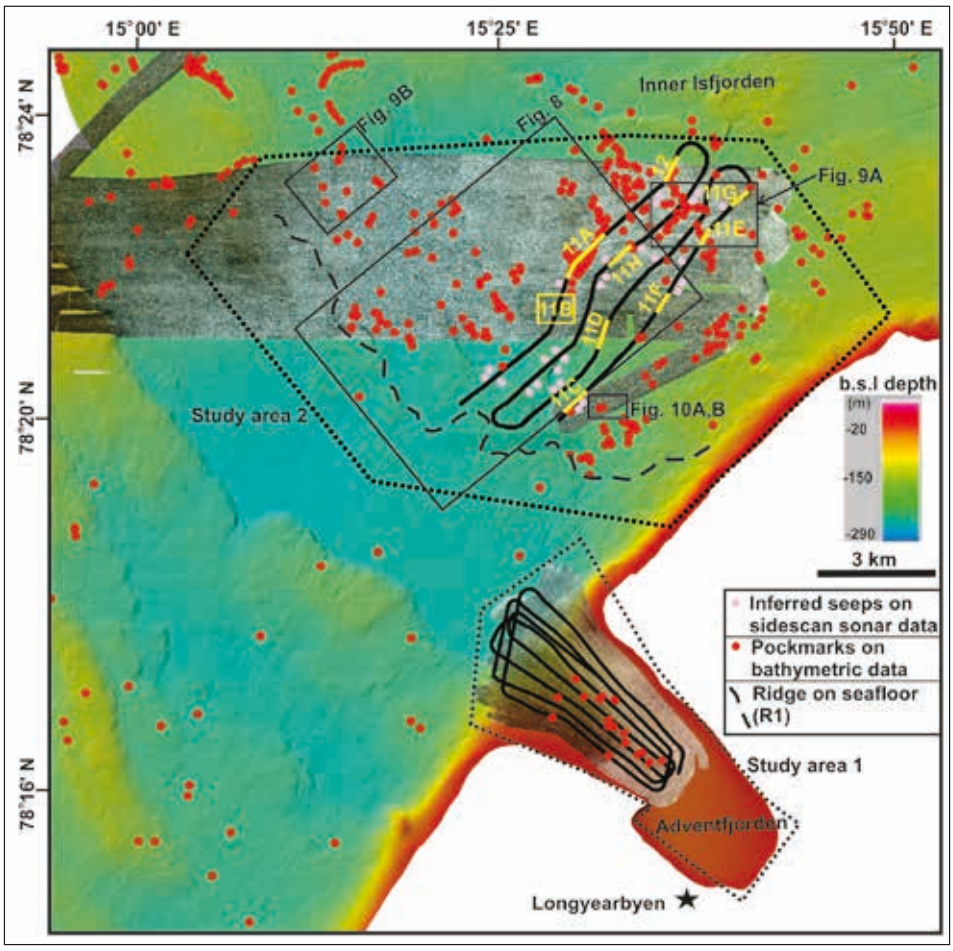

Figure 3. *Coverage of high-resolution multibeam bathymetric and backscatter data and sub-bottom acoustic profiles in the study area. Black lines show the ship track of sub-bottom acoustic profiles. Backscatter strength is shown in a grey tone where darker and lighter areas represent higher and lower acoustic backscatter values, respectively. Numbers 11 and 12 (in yellow) refer to figure numbers shown later.*

The multibeam backscatter data were collected from selected areas using a 30 kHz Kongsberg Maritime EM300 multibeam echo sounder onboard RV Helmer Hanssen in 2010 (Fig. 3). The raw data were processed using the Geocoder algorithm in IVS Fledermaus 7.0. The Geocoder algorithm removes the gains used during acquisition and applies a series of radiometric and geometrical corrections to the original acoustic observations in order to obtain corrected values of backscatter strength (Fonseca & Mayer, 2007). References to 'backscatter' in this paper should be regarded as relative (descriptive) backscatter strength.

Sub-bottom acoustic data

The sub-bottom profilers used in this study are capable of imaging the shallow sequences immediately below the hard, glacially influenced seafloor with a very high resolution. Two types of equipment were used to collect sub-bottom acoustic profiles in SA1 and SA2 (Fig. 3). A hull-mounted 4 kW EM 3300 sub-bottom profiler was used from the RV Helmer Hanssen in SA1. This instrument uses a frequency range of 2–16 kHz that allows a vertical resolution of 6–10 cm. The maximum penetration depth achieved in SA1 was 25 m.

SA2 has been surveyed in 2012 with the EdgeTech 2000–CSS, equipped with a sub-bottom profiler operating with a frequency range of 500 Hz to 12 kHz. It was deep-towed from the UNIS boat Viking Explorer. The maximum penetration depth achieved in SA2 was 12 m. Sound velocity profiles were collected at both SA1 and SA2 in order to convert travel times to metres in the acoustic profiles. Edgetech Discover II software was used for visual interpretation of the sub-bottom acoustic profiles.

Sidescan sonar data

Sidescan sonar records collected with EdgeTech 2000–CSS and simultaneously with the sub-bottom acoustic profiles were used to identify geomorphological features on the seafloor. The sidescan sonar is particularly important for seafloor surveys and seep studies because it can image regions of anomalous reflectivity that may be related to fluid expulsion, coarse seabed sediments, hard seafloor such as bedrock outcrops facing the sidescan source, gas hydrates, or methane-derived authigenic carbonates (Hovland & Judd, 1988; Orange et al., 2002; Collier & Brown, 2005).

Offshore 2D seismic data

The 2D multichannel marine seismic data used in this study comprise several 2D seismic surveys acquired by Statoil in 1988 and by the University of Bergen during the Svalex field course conducted between 2004

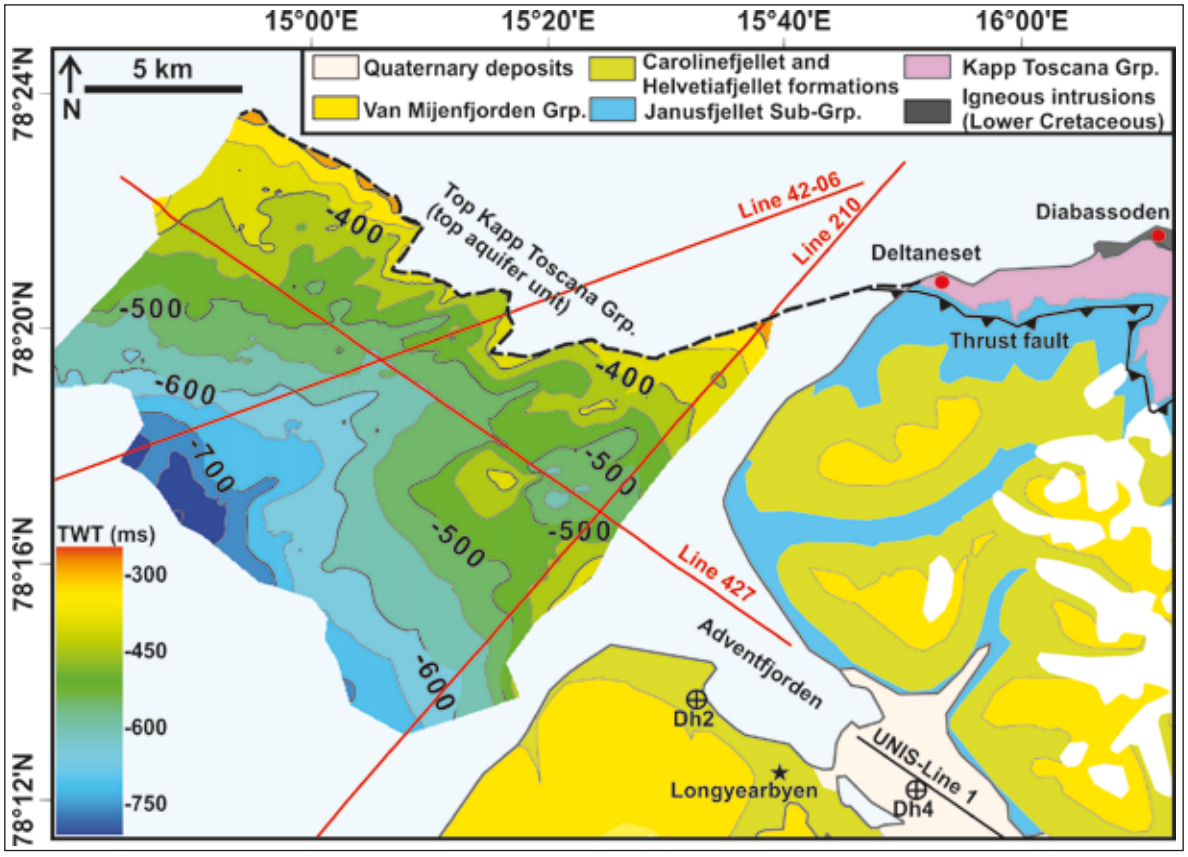

Figure 4. Map of the study area with the location of the three 2D multichannel seismic profiles. The TWT (two-way-travel time) map shows the subsurface depth of the Top Kapp Toscana Group (aquifer) interpreted on the seismic database. The bedrock geology map is based on Dallmann et al. (2002).

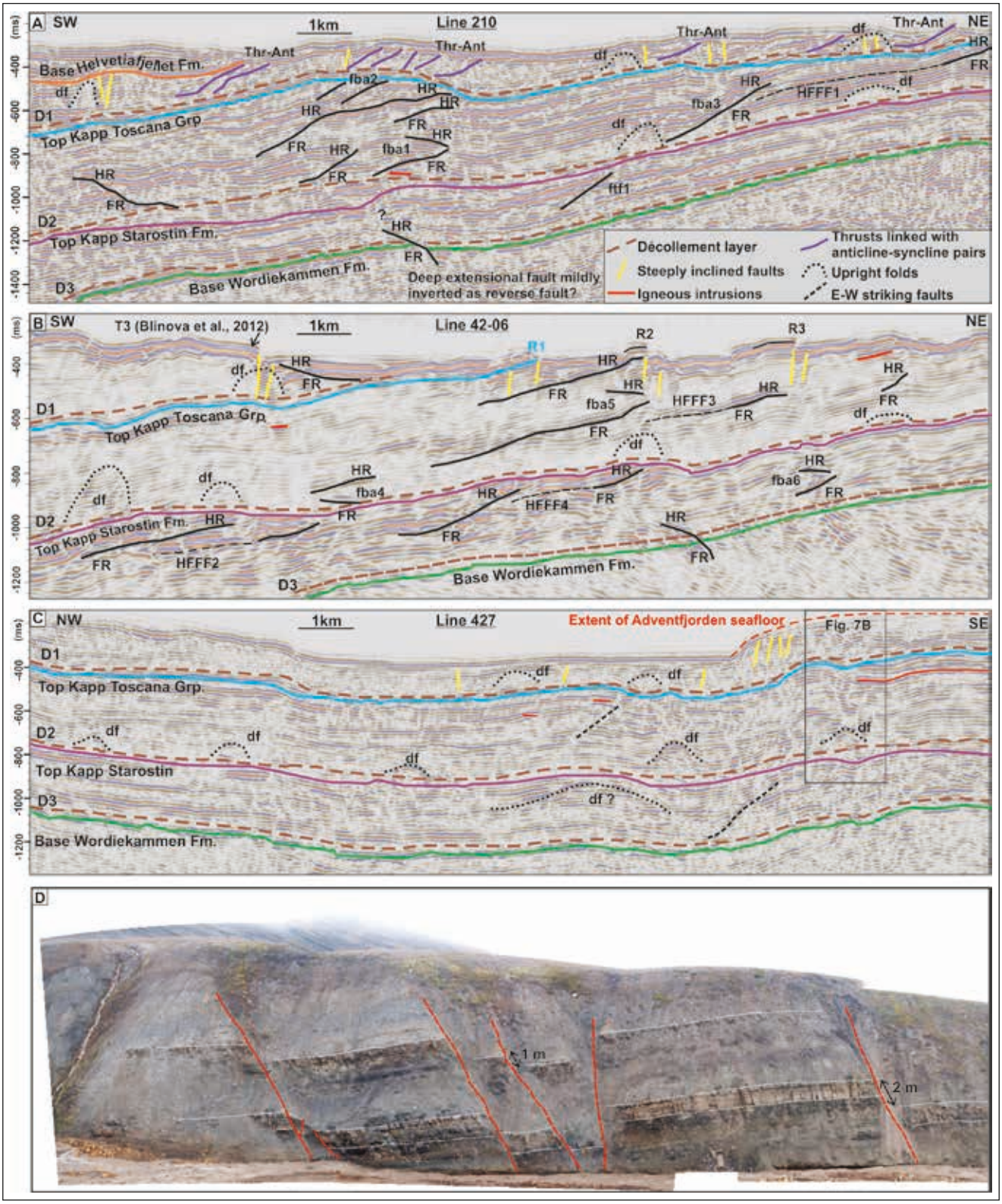

Figure 5. (A) 2D Seismic Line 210. (B) 2D Seismic Line 42–06. (C) Cross-profile 2D seismic Line 427. Seismic correlation is based on the stratigraphic table provided in Fig. 2B. D1, D2 and D3 are décollement layers. (D) Interpreted faults on a section of the upper part of the Kapp Toscana Group illustrated on outcrop near Deltaneset. Refer to Fig. 4 for seismic profile locations. HR – hangingwall ramp, FR – footwall ramp, HFFF – hangingwall – footwall flat, ftf – Fault-tip fold pair, df – detachment fold-thrust system, fba – long fault-bend anticline. ,Thr-Ant - see text for explanation. An un-interpreted version of the seismic profiles is shown in the Electronic Supplement.

and 2007. Details on the acquisition and processing parameters of the 2D seismic data are given in Blinova et al. (2012) and Bælum & Braathen (2012). The dataset of the entire fjord is of mixed quality, with parts especially distorted by pegleg multiples caused by the hard seafloor (Digranes & Kristoffersen, 1995; Bælum et al., 2012). Acoustic penetration generally enables a distinction of reflectors to depths of 3–4 seconds TWT (two-way travel time). Identification of geological unconformities and fault interpretation were carried out on the whole seismic dataset. Structural interpretations are illustrated on three selected seismic profiles: Line 210, Line 42–06 and Line 427 (Figs. 4, 5).

Onshore 2D seismic data

The onshore seismic data were collected with a 60 channel 1500 m snow streamer pulled by a bandwagon. The source used was dynamite (Dynacord) with charges of 2–4 kg per shot. The onshore data quality is not optimal due to the high noise-to-signal ratio resulting from the coupling of towed geophones with the ground. Other factors influencing the quality of the data are wind, composition of the snow layer, and noise from motor vehicles and infrastructure (e.g., snow scooter traffic, electrical lines) (Bælum et al., 2012). The geological interpretation of the seismic dataset and the tie with the borehole Dh4 was done using Petrel software (Fig. 6).

Results and interpretation

2D multichannel seismic profiles

Interpretation of the stratigraphic units on the 2D MCS (multi-channel seismic) data is based on the seismic reflection interpretations of Bergh et al. (1997), Bælum et al. (2012) and Blinova et al. (2013). The three medium- to high-amplitude, consistent reflectors identified in the upper part of the seismic profiles are: (1) near the top of the Wordiekammen Formation (base Upper Carboniferous), (2) near the top of the Kapp Starostin Formation (Upper Permian or base of the Triassic shales), and (3) near the top of the Kapp Toscana Group (Upper Triassic–Middle Jurassic) (Fig. 5A, B, C). Other strong reflectors such as the base of the Helvetiafjellet Formation and the base of the Palaeogene succession (Firkanten Formation) could also be identified regionally, but are not further discussed in this study. Seismic facies analysis and interpretation of the geological groups and formations are presented in Table 1.

The strong and continuous seismic reflector of the near-top Kapp Toscana Group was used to produce a time-structure map for analysis of the structural domains and styles in the study area (Fig. 4). The generated surface dips gently to the SW at 2–3°. The near-top Kapp Toscana Group has a depth of 700 ms (TWT) (equivalent to *c.* 1400 m) in the offshore setting, 11.5 km northwest of the planned injection site in Longyearbyen. The unit reaches the seafloor *c.* 13 km northeast of the injection site (Fig.

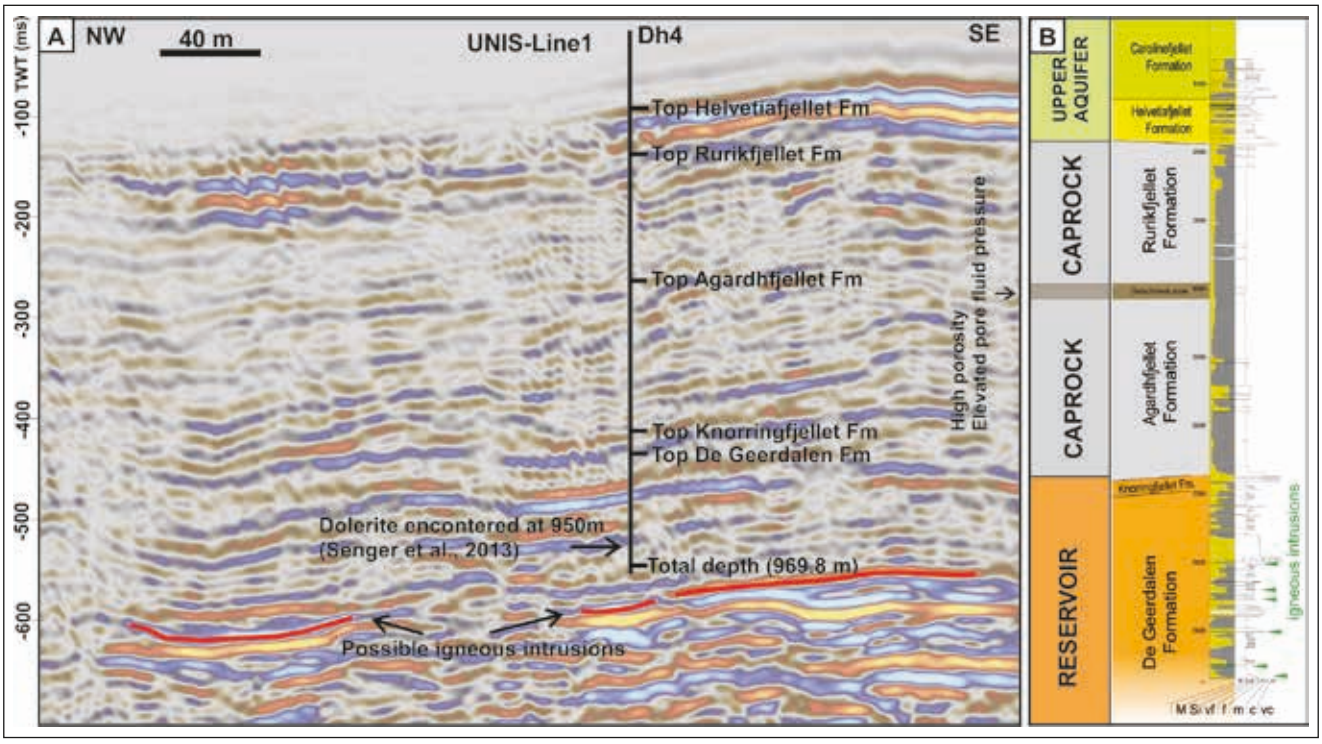

Figure 6. *(A) Onshore seismic UNIS-Line 1 tied with (B) Dh4 lithology log based on Ogata et al. (2012). Locations of UNIS-Line 1 and Dh4 are shown in Fig. 4. Igneous intrusions have been interpreted on adjacent seismic lines by Bælum et al. (2012). Note that the scale of the lithology log presented on the right-hand side does not coincide with the formation markers on the Dh4 log shown on the seismic data.*

Table 1. *Characterisation of seismic units identified in the offshore multichannel 2D seismic dataset (Fig. 5A, B and C). Interpretation of the geological units is based on Bergh et al. (1997), Bælum & Braathen (2012) and Blinova et al. (2013).*

Seismic characteristics of units	TWT thickness (ms)	Inferred lithology (age)	Observed fold-thrust belt structures
Low-amplitude and discontinuous reflectors overlain by thick bed of high-amplitude continuous reflectors.	180–200	Janusfjellet Group shales overlain by Helvetiafjellet Fm. sandstones. (Upper Jurassic–Lower Cretaceous)	NNW–SSE-striking, gently dipping thrusts associated with anticlines splay from décollement layer. Steep, small faults and upright folds linked to blind thrusts as well as E–W-trending faults reach the seafloor.
Discontinuous, very low-amplitude reflectors, overlain by thick bed of high-amplitude continuous reflectors interlayered by thin transparent layers.	360–380	Shale and sandstone layers of the Sassendalen and Kapp Toscana groups. (Lower Triassic–Middle Jurassic)	NNW–SSE-striking gently dipping thrusts, upright folds above the décollement layer and rare occurrence of E–W-trending faults.
High-amplitude, continuous reflectors with rare, thin transparent layers in between.	280–300	Sandstone, carbonates and evaporites of Tempelfjorden and Gipsdalen groups (Upper Carboniferous–Permian)	Few NNW–SSE-striking thrusts and uncertain E–W-trending faults above the décollement layer.
Low-/medium-amplitude, discontinuous scattered reflectors with various signal intensity.	----	Clastic sedimentary rocks (Devonian–Middle Carboniferous)	----

4). Correlation of the Dh4 borehole with onshore seismic line UNIS–Line 1 marks the top of the Kapp Toscana Group (Knorringfjellet Formation) at 450–500 ms (TWT), corresponding to *c.* 670 m depth (Fig. 6).

Very strong horizontal reflectors with abrupt reflection terminations and discordant relationships with stratal reflections have been interpreted as igneous intrusions within the Kapp Toscana Group (Figs. 5, 6). High-amplitude reflections indicate a significant difference in acoustic impedance between igneous material and the sedimentary host rocks. It is a typical seismic signature of igneous intrusions (Hansen et al., 2004; Bælum et al., 2012; Senger et al., 2013).

Structures related to the fold-and-thrust belt

Interpretation of fold-and-thrust belt structures follows the principle of conservation of length, in which beds that are thrusted and folded should be restorable to a viable configuration (Boyer & Elliott, 1982; Woodward & Rutherford Jr., 1989). In our study, we have identified dip-domains that are well illustrated by large and long fold limbs that terminate at certain levels. Examples are given by the gentle fault-bend anticlines labelled *fba1* to *fba3* in Line 210 and *fba4* to *fba6* in Line 42–06 (Fig. 5A, B). From the overall fold geometry a basic sequence of folding and thereby thrusting can be inferred. The *fba2* anticline is better developed than *fba1*, suggesting that the former anticline was refolded when the *fba1* anticline grew, consistent with a foreland-breaking sequence of deformation. The *fba3* anticline sits above a regional low-angle thrust with an interpreted ramp-flat-ramp geometry, which represents the basal structure of this area farther northeast.

Thrust flats have been interpreted by identifying areas of inconsistent dip and thereby defining possible hangingwall and matching footwall ramps. The best example is the *HFFF1* shown in Line 210 to the northeast and *HFFF2* to *HFFF4* in Line 42–06 (Fig. 5A, B). The folds associated with the flat-ramp thrust system were accordingly analysed, with respect to a fault-bend fold fitting ramp geometries and fault-propagation folds, thus suggesting tighter structures. The latter can be observed in Line 210, specifically *ftf1*, where a transparent zone above a thrust ramp could be a fault-propagation fold pair with a steep forelimb. A steep forelimb would cause limited or no reflection and thereby nearly transparent seismic signatures.

Three décollement layers could be outlined on the seismic dataset from which several major thrusts spread out (Bergh et al., 1997; Blinova et al., 2012). Typical for the top two décollement layers are local zones with a series of more or less upright folds linked to small, blind thrusts (Maher et al., 1986). Their size and geometry are challenging to constrain in the seismic data. Some of these structures are indicated on the seismic profiles, labelled *df* (Fig. 5A, B, C).

Gently to steeply dipping, strong reflectors (labelled as *Thr-Ant*) splay from the décollement within the Janusfjellet Subgroup shales in the topmost part of Line 210 (Fig. 5A) and in other seismic profiles in the study area. These features are interpreted as thrusts linked to overlying anticline-syncline pairs within the organic shales, located close to the seafloor. Several small, steeply inclined faults (marked with yellow lines) are interpreted in the topmost part of the seismic profiles Line 210 and 42–06 (Fig. 5A, B). They cut up to the seafloor and are rooted in the Kapp Toscana and Adventdalen groups. With roots in the upper décollement and closely associated with thrust zones and upright folds, we suggest that they formed at the same time as the fold-and-thrust

belt complex. However, as these steep faults offer fault offsets of less than 40–50 m, they are difficult to resolve in the seismic data. In this context, outcrop field data from Deltaneset confirm the presence of small offset (1–2 m) faults in the upper part of the Kapp Toscana Group (Fig. 5D). These structures are best seen in, for instance, Line 427, which is parallel to the Tertiary structural trend of the fold-thrust belt. It allows analysis of other possible fault sets oriented at a high angle to the fold-thrust structures, which have been described in the literature (Braathen & Bergh, 1995; Bergh et al., 1997; Braathen et al., 1999). Similar to the steep faults mentioned above, a set of faults associated with reflector truncations has been interpreted in the Tempelfjorden, Sassendalen, Kapp Toscana and Adventdalen groups. The identified faults have small vertical offsets (within seismic resolution), and appear as vertically segmented fault arrays on the 2D seismic profiles. These faults have a different strike as compared to the NNW–SSE-trending fold-thrust system, but their specific orientation is hard to establish as these structures are not easily correlated between adjacent seismic profiles. Their strike is, however, within the NE–SW to E–W sector. This is substantiated by observations of many, nearly E–W-oriented, steep normal and oblique-slip faults in the coal mines in the Paleocene succession (Jochmann, pers. comm.), which shows a clear linkage with thrusts. In light of this dataset and the mentioned literature, the described faults are most likely either transfer oblique-slip faults or extensional faults (Braathen & Maher, 1995), linked to stress driving the folding and thrusting. The upright folds linked to blind thrusts (labelled as df) rooted in the top two décollement layers are also observed in Line 427. A large anticlinal fold spreading over 2 km is interpreted in the Upper Permian Tempelfjorden Group. This structure is interpreted as a lateral-ramp anticline, caused by variation in ramp dip and variations in thrust displacement during the contractional event.

Multibeam bathymetric data

The water depth in SA1 varies from 17 to 160 m from head to mouth, respectively (Fig. 7A). The seafloor is relatively smooth near the head as compared to the central part and mouth of the fjord. Water depth in SA2 varies from 220 to 300 m. Sub-parallel ridges with 5–20 m relief and striking NNW–SSE are identified on the bathymetric data in SA2 (Figs. 8, 9).

Pockmarks of various size and shape have been identified on the bathymetric data in both study areas (Figs. 7A, 10) (Forwick et al., 2009). Diameter, depth and the water depth at which they occur are presented in Table 2. Their shapes range from circular to elongate. Unit-pockmarks (1 to 5 m diameter; depth <0.6 m) are observed in the vicinity of normal-sized pockmarks (Fig. 7A). Unit-pockmarks have been described as circular depressions on the seafloor (diameter <5 m), usually found as singular features or in the form of strings or clusters (Hovland et al., 2010). Pockmarks occur in the central and outer parts of SA1, whereas they are found to be mostly aligned along the troughs associated with NNW–SSE-trending ridges in SA2 (Fig. 9). Unlike other parts of the Isfjorden fjord system, glacial lineations and other submarine landforms on the seafloor relating to glacial activities are absent in both SA1 and SA2 (Roy et al., 2012).

Integrated analysis of 2D seismic and bathymetric data suggests that the NNW–SSE-trending R1 ridge is the near-top of the Kapp Toscana Group sub-cropping at the seafloor. The ridges labelled as R2 and R3 relate to thrust faults associated with upright folds sub-cropping on the seafloor, spreading from the décollement layer in the Sassendalen Group shales (Figs. 5B, 8). Similarly aligned ridges in the vicinity are interpreted as anticline-syncline pairs linked to thrusts, sub-cropping on the seafloor (Fig. 9).

Multibeam backscatter data

The multibeam backscatter (BS) covers 15 km^2 and 72 km^2 of SA1 and SA2, respectively (Fig. 3). The seafloor BS has values ranging from 0.23 to -54.26 dB (mean value of -26 dB and standard deviation of 3.24) in SA1 and -11.42 to -60.24 dB (mean value of -30.24 dB and standard deviation of 2.47) in SA2. Higher BS values are observed in the western part of the fjord as compared to the eastern part. A backscatter profile across the pockmarks, identified on the bathymetric data, shows low backscatter anomalies in comparison to the surrounding seafloor BS values (Figs. 7C, D, 10A, B).

High seafloor BS values could result from either a harder seafloor or coarse-grained sea-bottom sediments. Low BS values associated with pockmarks in this study are assumed to result from enhanced porosity contrasts

Table 2. *Morphological characterisation of pockmarks and the water depth in which they occur in the two study areas. Please note that the total pockmark count mentioned here does not include unit-pockmarks. (Avg. – average; S.D. – Standard deviation).*

Region name	Total pockmarks	Diameter (m)			Depth (m)			Water depth (m)
		Range	Avg.	S.D.	Range	Avg.	S.D.	
Study area 1	17	20–114	83.18	20.98	1–7	2.82	1.72	70–120
Study area 2	381	10–213	41.57	28.82	1–7	1.66	1.00	169–270

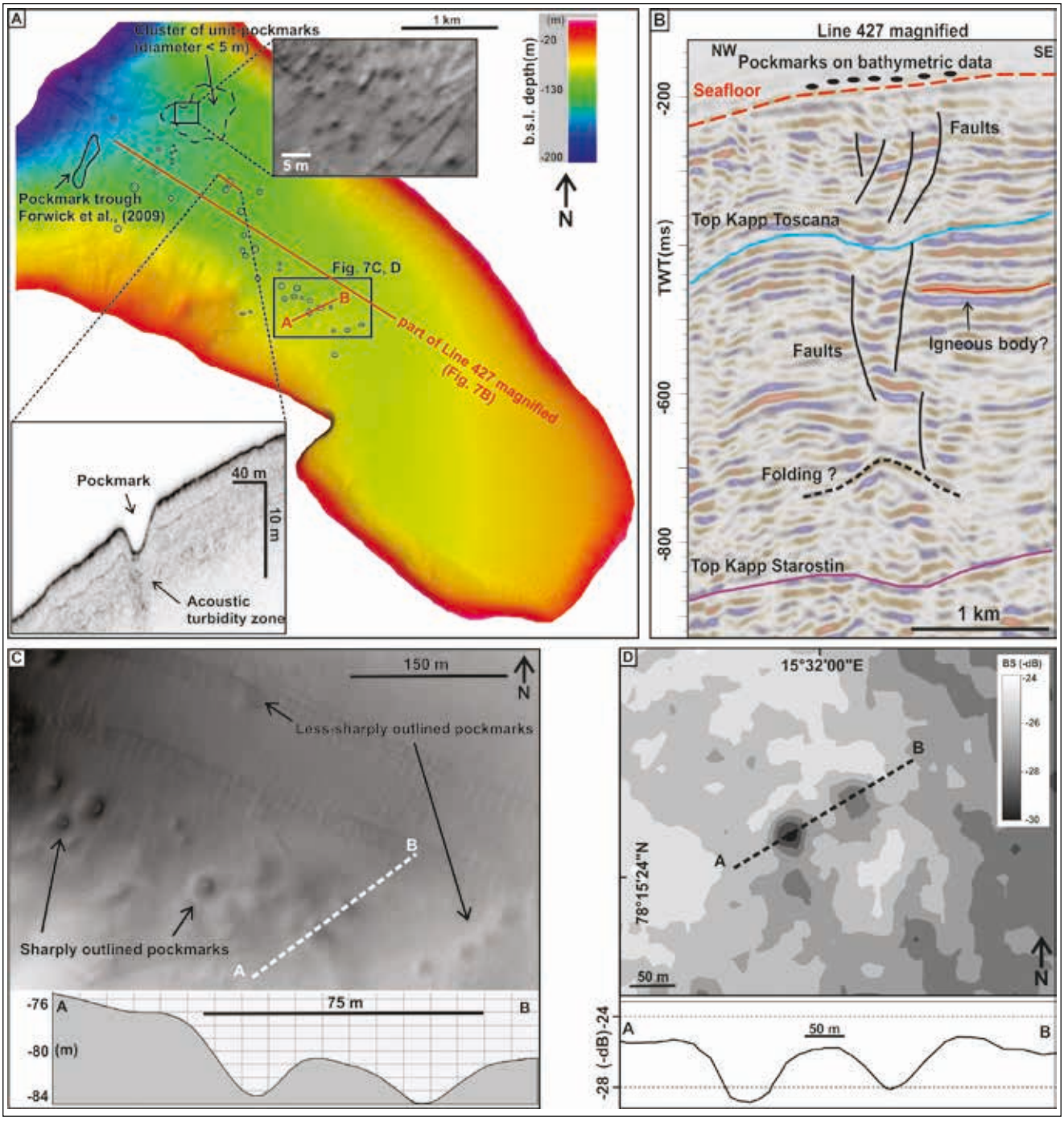

Figure 7. *(A) High-resolution multibeam bathymetric data from SA1 (Adventfjorden) showing the distribution of pockmarks. The area enclosed by the dashed lines in the northwest of the fjord has c. 25–30 unit-pockmarks (top inset shows magnified unit-pockmarks on bathymetric data). Bottom inset illustrates the acoustic turbidity zone beneath a pockmark on the sub-bottom profile. (B) Structural interpretation of 2D seismic data (Line 427) in deeper successions beneath the pockmarks. (C) Sharply and less-sharply outlined circular pockmarks. Profile A–B across the pockmarks is illustrated beneath. (D) Multibeam backscatter data and corresponding A–B profile across the same pockmarks shown in Fig. 7C.*

by trapped overpressured fluids/gas in the shallow sediments beneath the pockmarks, or possibly due to their crater-like morphology.

Sidescan sonar data

Twenty-seven circular patches of high backscatter values were recorded with the sidescan sonar in SA2 (Figs. 3, 11B). Their diameter ranges from 5 to 15 m. They occur in the vicinity of the high-density pockmarked seafloor, mapped on the bathymetric data. A set of randomly distributed striations was observed on sidescan sonar records.

The presence of coarse-grained sediments or a hard seafloor will produce high backscatter on the sidescan records. However, their circular shapes suggest that

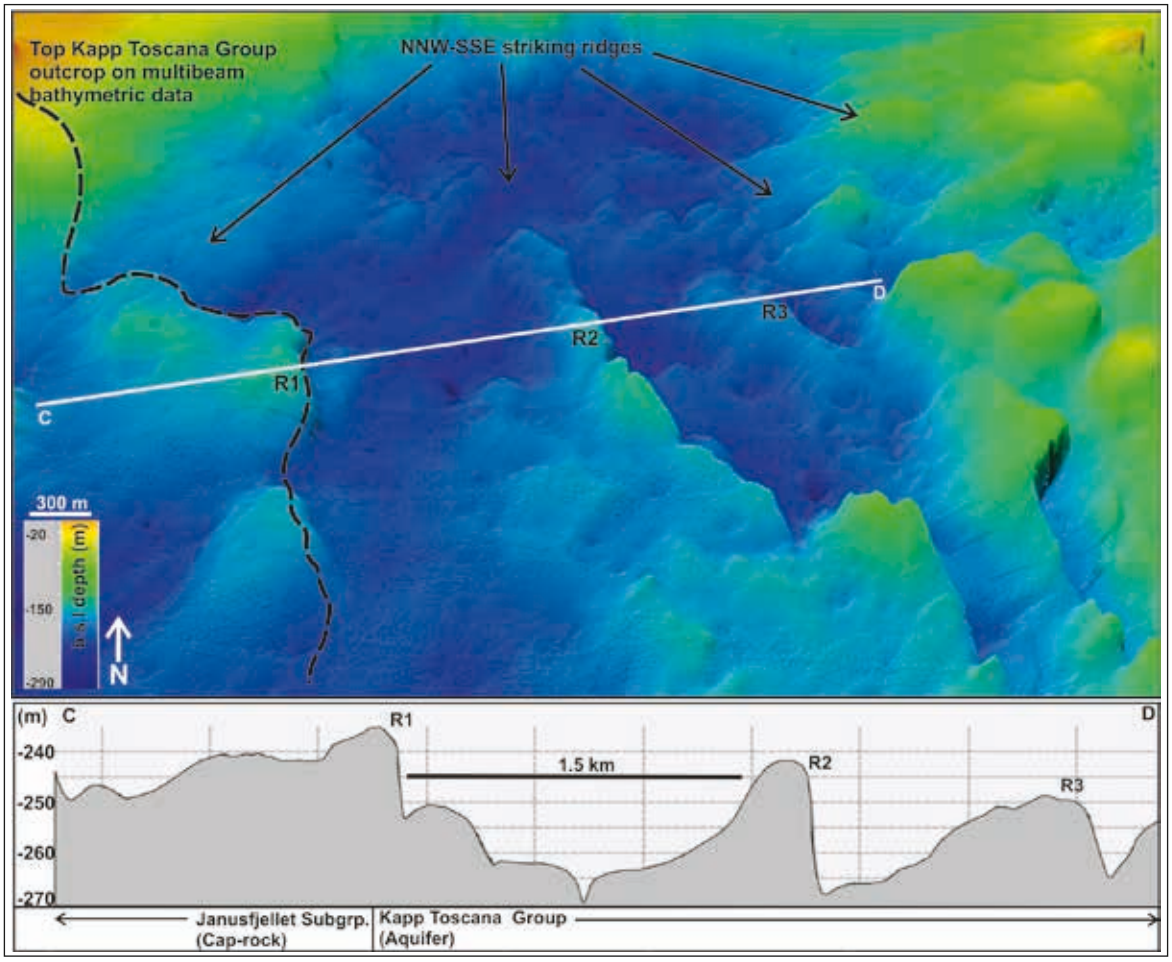

Figure 8. High-resolution multibeam bathymetric data from SA2 illustrating the NNW–SSE-striking ridges on the seafloor, tied to interpretation of seismic Line 42–06 (Fig. 5B). Location is shown in Fig. 3. The ridges are seafloor expressions of the top of the Kapp Toscana Group and upright folds and blind thrusts relating to the fold-and-thrust complex. Refer to text for details. Profile C–D illustrates the dimensions of the ridges.

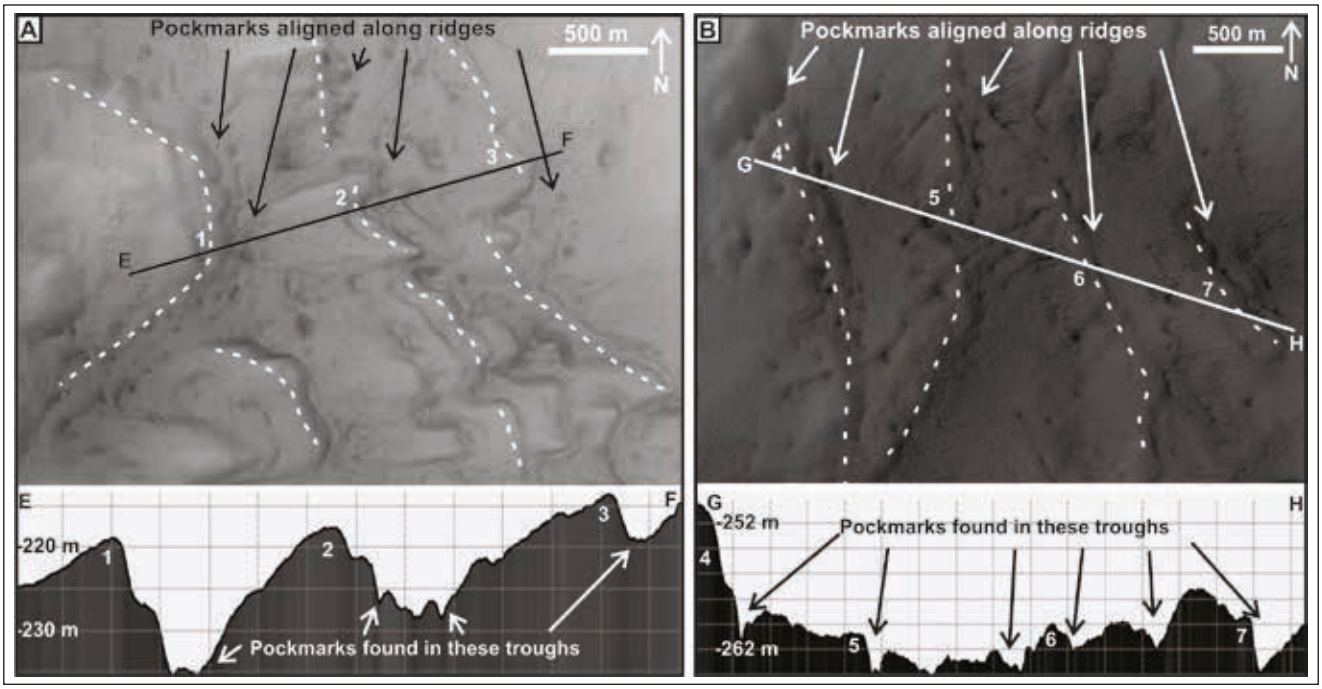

Figure 9. High-resolution bathymetric data illustrating the alignment of pockmarks along ridges in inner Isfjorden. The pockmarks are preferentially located in the troughs associated with the ridges. The ridges are marked as numbers 1 to 7 on the bathymetric data as well as in their corresponding cross-profiles E–F and G–H; interpreted as sub-crops of Triassic – Lower Jurassic bedrock and thrust faults after tying with the seismic dataset. Locations are shown in Fig. 3.

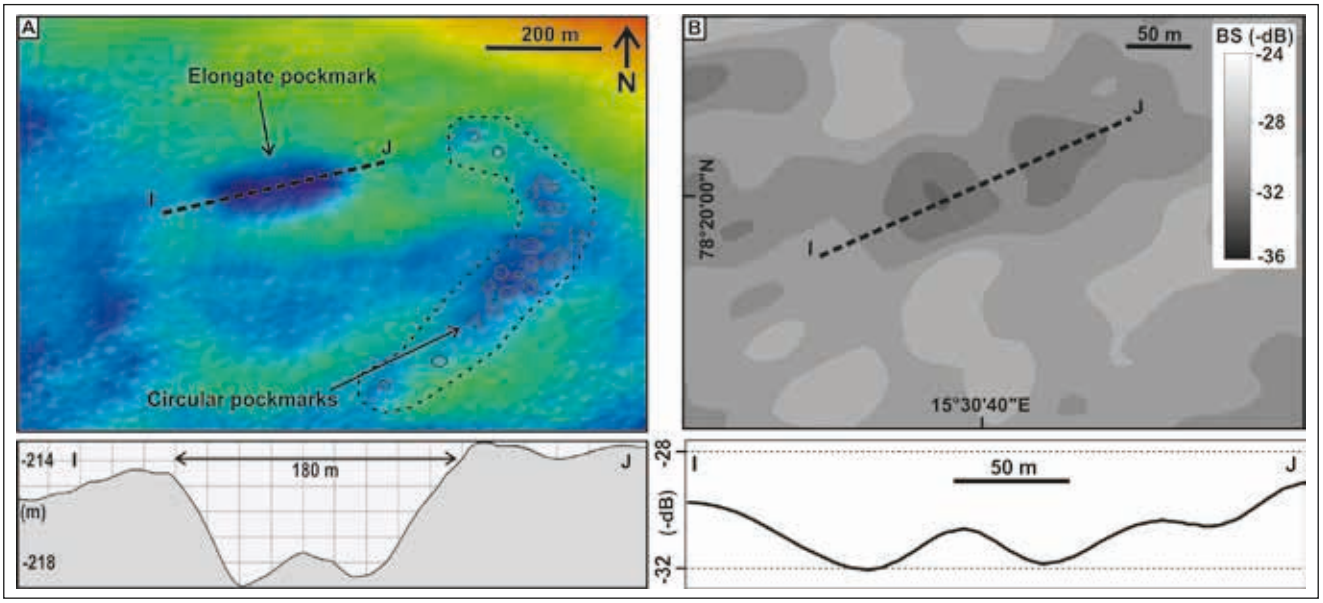

Figure 10. *(A) High-resolution bathymetric data showing the morphology of an elongate pockmark and distribution of smaller circular pockmarks. (B) Multibeam backscatter data from the same elongate pockmark as shown in (A), showing a low backscatter anomaly from the centre of the pockmark. Profile I–J beneath illustrates the vertical profile across the same elongate pockmark in both cases. Location is shown in Fig. 3.*

they are more likely related to focused seepage of fluids through the seafloor. The high density of organisms, shell fragments or authigenic carbonates usually found at seep sites result in such high backscatter anomalies. The circular patches of high backscatter are possibly caused by the presence of coarse-grained sediments or shell fragments left after fluid seepage. Hence, we interpret them as inferred seep locations. Similar observations have been made by Hovland & Judd (1988) in the North Sea and by Orange et al. (2002) in the California margin. We could not observe any striations on the bathymetric data as recorded on the sidescan records (Fig. 11B). The absence of these striations on the bathymetric data suggests that they are not related to any geological features, but rather possibly related to interference from other instruments recorded on the sidescan data.

High-resolution sub-bottom acoustic data

Four seismo-stratigraphic units were identified on the sub-bottom acoustic profiles in SA2 based on their relative reflectivity strength and acoustic signature (Table

Table 3. *Seismic facies analysis of shallow stratigraphic units in SA2 (Fig. 11A). The lithologies and chronostratigraphy are based on Forwick & Vorren (2010).*

Unit	Observations: acoustic characteristics	Thickness and extent	Lithology/ chronostratigraphy	Observed acoustic anomalies
A4	Coherent medium backscatter within the unit bounded by medium-/high-amplitude base reflector. The unit shows high backscatter in the southern part.	Thickness of 2–4 m. Rests over A3.	Mid to late Holocene heterogeneous glacimarine.	Local high-reflective patches and acoustic turbidity zones below pockmarks. (Figs.7A, 11E)
A3	The top reflector is of medium-/high-amplitude and the base reflector is of low-/medium-amplitude diffuse signature. Low-/medium-amplitude in order to keep consistency with restcoherent backscatter within the unit.	2–4 m thick. Thickness increases from south to north. Rests on A2.	Early Holocene, relatively uniform, fine glacimarine deposits.	Local high-reflective patches. (Fig. 11H)
A2	The lower- and upper-bounding reflectors are of low-amplitude diffuse nature. Low-amplitude coherent backscatter within the unit with 2–3 internal reflections.	5–8 m thick. Overlies A1 in general. Relatively thicker in southern part.	Late Weichselian–earliest Holocene glacimarine deposits. Internal reflectors indicate lithological variations within deposits.	Turbid zones spreading from A1 in some cases. (Fig. 12)
A1	Acoustically opaque layer with medium-/high-amplitude incoherent backscatter. Discontinuous, upper-bounding reflector, base reflector has low to medium continuity representing acoustic basement.	Thickness varies from 2–10 m. Sequence affected by faults. Overlies bedrock.	Late Weichselian–earliest Holocene subglacial deposits.	Discontinuous upper bounding reflector is affected by vertical acoustic blankings and turbid zones. (Figs. 11A, C, D, 12)

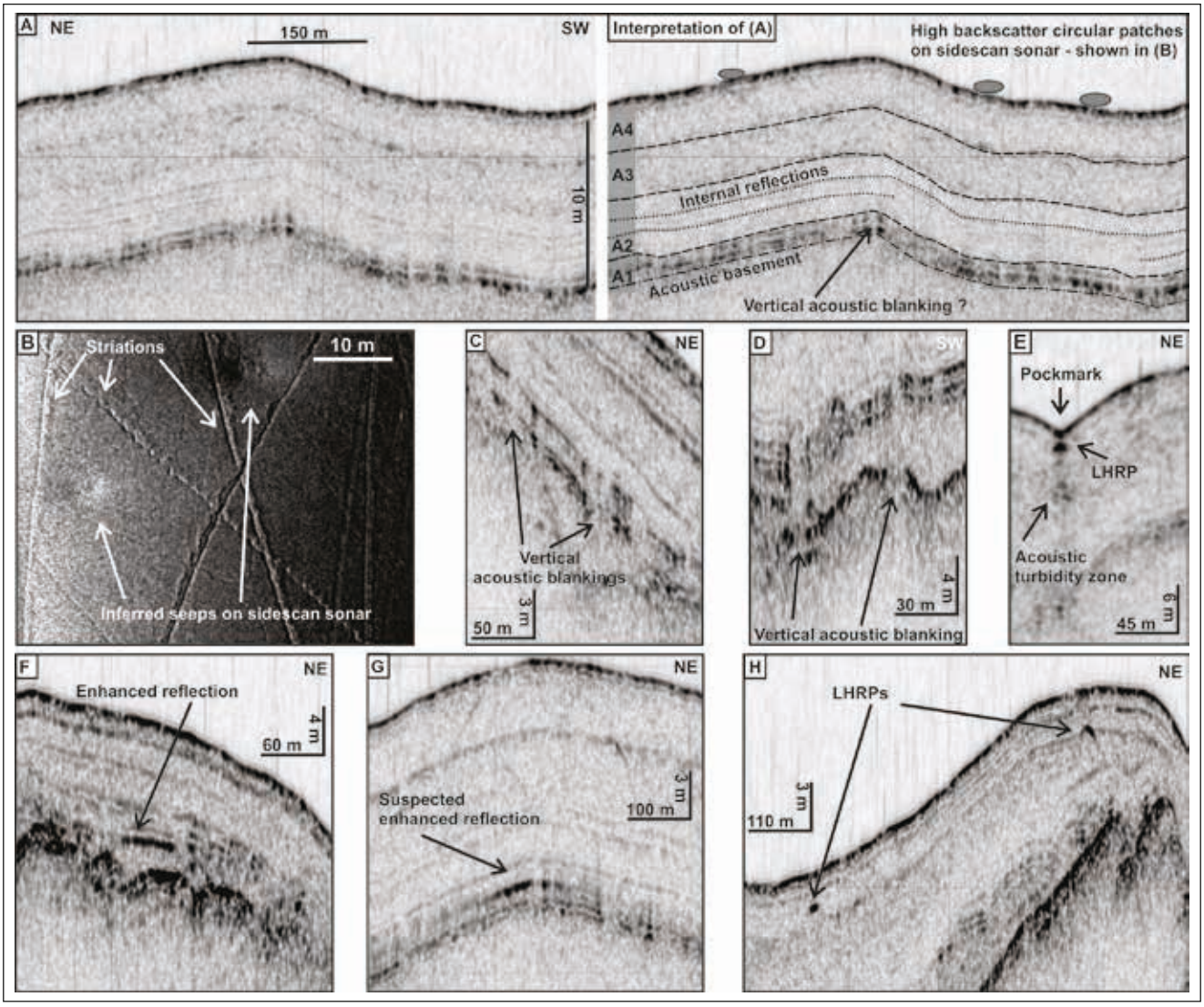

Figure 11. *(A) Sub-bottom acoustic data from SA2 showing the four, shallow seismo-stratigraphic units. Refer to Table 3 for acoustic facies analysis and lithology interpretation. (B) High backscatter circular patches recorded on the sidescan sonar data. The striations seem to be artifacts resulting from interference of other signals. (C, D) Vertical acoustic blankings imaged within Unit A1. (E) Acoustic turbid zone and a local high-reflective patch (LHRP) beneath a pockmark. (F, G, H) Enhanced reflections and LHRPs. Locations are shown in Fig. 3 with yellow labels.*

3, Fig. 11A). The units are bounded at the base and top by laterally semi-continuous, parallel to sub-parallel, variable amplitude seismic reflectors. However, the lateral continuity of these sedimentary units is locally distorted by the presence of acoustic blanking and turbid zones. The top of the acoustic basement could be interpreted in most of the study area. It is characterised by a medium- to high-amplitude and low to medium continuity. It is imaged as a partly diffuse reflector draping the morphology of the bedrock. Low- to medium-amplitude diffuse reflectors bound relatively thin units (<1 m thick) at the mouth and thicker units towards the head of Adventfjorden. Based on their acoustic signatures, three major types of acoustic features have been interpreted which are assumed to be related to the occurrence of shallow gas.

Vertical acoustic blankings

Acoustic transparent columnar disturbances are observed within Unit A1. They are typically 2–4 m high and appear as columnar patches distorting the coherency and continuity of the seismo-stratigraphic unit and its bounding seismic reflectors (Fig. 11A, C, D).

This effect on the sub-bottom acoustic profiles could be caused by most of the acoustic energy being reflected from the top of the transparent acoustic column by hard sediments, or by some physical condition within the sediment column. The presence of gravels or a similar sediment type could cause scattering of acoustic energy, whereas interstitial gas could absorb the energy. Similar columnar acoustic features usually occur in marine sediments from the disruption of sediment layering by the upward migration of gas dissolved in pore water. We suspect that fluids migrating vertically through Unit A1

may have been responsible for these vertical acoustic blankings. They could be interpreted as gas chimneys representing zones of focused upward migration of gas. However, their origin is uncertain. Similar acoustic features are referred to as 'acoustic fountains' by Hovland & Curzi (1989) in the Adriatic Sea, representing homogeneous columns of relatively high-pressured pore water containing a high concentration of dissolved gas or micro-bubbles migrating upwards.

Acoustic turbidity

Acoustic turbid zones appear as chaotic reflections resembling a dark smear on the sub-bottom acoustic profiles. They are usually found beneath pockmarks occasionally in SA1 and SA2, but the top of the turbid zone is not prominent (Figs. 7A, 11E). They also occur within units A1 and A2 near the troughs associated with bedrock ridges mapped on the bathymetric data (Fig. 12). The acoustic turbid nature of sediments could result from a dense population of highly reflective or scattering elements within the sedimentary units. Absorption of acoustic energy by gas-charged sediments beneath pockmarked areas in the North Sea has been reported to have resulted in a similar acoustic signature (Hovland & Judd, 1988). Hence, it is suspected that the turbid zones beneath the pockmarks in Unit A4 represent gas-charged sediments where the pores in the glacimarine sediments are partly filled with pore water and partly filled with free gas. However, the concentration of free gas in such acoustic turbid zones could be very low (0.5–2% by volume) (McQuillin et al., 1984; Wilkens & Richardson, 1998). The lack of a prominent upper boundary of the turbid zones beneath the pockmarks might be due to minor seepage near the seafloor.

The acoustic turbid zone is discordant to the acoustic facies of units A1 and A2 (Fig. 12). Reflections within Unit A1 are absent within the turbid zone, which can be explained by two possibilities. The reflections within Unit A1 could be masked by the presence of gas-charged sediments. Alternatively, the chaotic acoustic signature could be interpreted as positive landforms of glacial origin such as sediment wedges or recessional moraines (Forwick & Vorren, 2010). The steep sides of the moraines or wedges would practically scatter and reflect most of the acoustic energy, resulting in such a masked chaotic acoustic signature below. However, we suspect that this feature could also be related to sediment diapirism associated with differential vertical pressure zones and the occurrence of gas-charged sediments, as explained by Hovland & Curzi (1989). The gentle bulge at the seafloor above this acoustic turbid zone could have formed due to sediment diapirism which was possibly associated with accumulation and migration of dissolved gas bubbles in pore water after being expelled from the bedrock basement (marked as 'convection' in Fig. 12).

Enhanced reflections

Anomalous high-amplitude reflections with abrupt terminations and local high-reflective patches have been observed in several stratigraphic levels (Fig. 11E, F, G, H). They are usually found beneath pockmarks and inferred seep locations detected on sidescan sonar data.

Enhanced reflections are usually caused by strong contrasts in acoustic impedance due to lithological variations within the sedimentary units. The local high-reflective patches and hyperbolic reflections within the near-seabed sediments could be caused by point-source targets, like ice-rafted debris (IRD) and dropstones dropped by melting icebergs. However, it is common in shallow-marine sediments to find the presence of free gas (<1% of the pore volume) which causes a reduction in P-wave velocity and high impedance contrast, giving rise to a reflection with anomalously high amplitude from the top of the gas (Judd & Hovland, 1992; Schroot et al.,

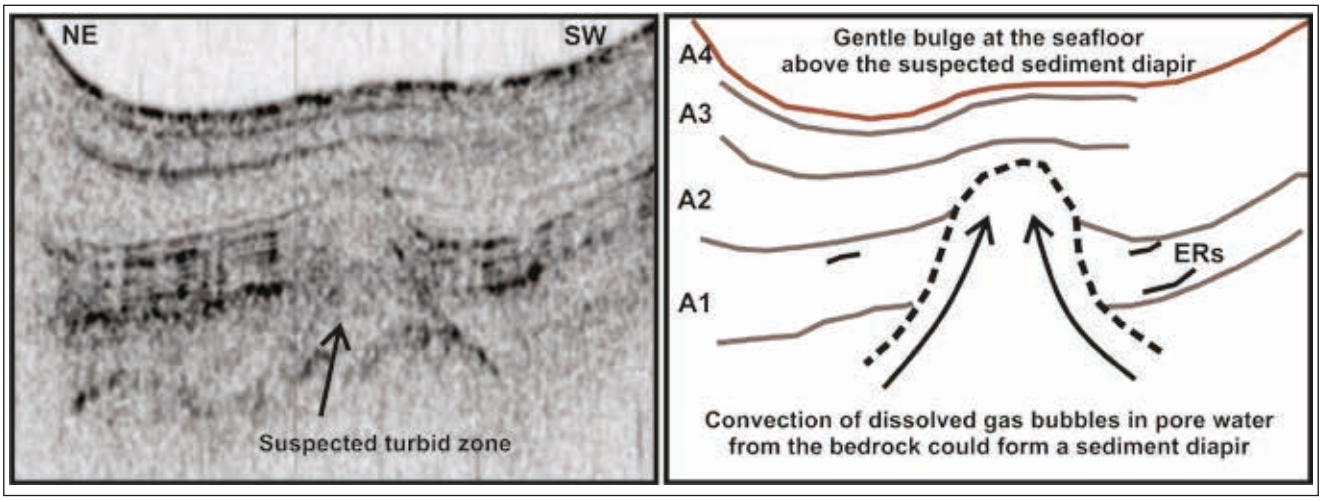

Figure 12. *Acoustic turbid zone in units A1 and A2 and its interpretation as a suspected gas-associated sediment diapir following a theory proposed by Hovland & Curzi (1989). The increase in thickness of Unit A1 to the right of the suspected diapir suggests probable injection of sediments from beneath. Location is shown in Fig. 3 with yellow label. ERs = Enhanced reflections.*

2005). Hence, we suspect that the enhanced reflections and local high-reflective patches were possibly caused by the local accumulation of minor amounts of free gas within porous sediments below a certain horizon.

Discussion

The integrated analysis of various high-resolution geophysical datasets investigated in this study provides the present distribution of pockmarks relating to natural fluid migration, where the succession of aquifer and cap rock crops out northeast of the Longyearbyen CO_2 injection site.

Present state of seabed seeps and shallow gas

Forwick et al. (2009) have reported sharply to less sharply outlined pockmarks along with composite pockmarks and pockmark troughs in Adventfjorden (SA1) (Fig. 7). We have found individual pockmarks (diameter 10–213 m, depth 1–7 m), clusters and individual unit-pockmarks (diameter <5 m) and pockmark strings in both study areas (Figs. 3, 7, 9). They represent passive fluid seepage from the seafloor. There is no direct evidence of ongoing seepage into the water column from the pockmarks. However, these locations could have greater potential for continuing or periodic fluid seepage. Unit-pockmarks usually represent the most recent and active local seep locations, based on observations made by Hovland et al. (2010) on the continental shelf off western Norway.

Comparison of bathymetric and sidescan sonar data produced mixed results. Circular patches with high backscatter values recorded on the sidescan sonar were inferred as seep locations (Fig. 11B). It is less likely, but possible, that the existence of sidescan circular patches was caused entirely by subsurface features, for example gas bubbles a few metres below the bottom, with no recognisable expression on the sub-bottom acoustic profiles. There are a number of processes that would increase backscatter from a seep location (Hovland & Judd, 1988; Orange et al., 2002). Such effects associated with seabed seeps include authigenic carbonate nodules, gas bubbles and residual coarse sediments left behind from fluid eruptions and unit-pockmarks. These inferred seeps on the sidescan sonar data were not identified on the bathymetric data, which were acquired four years before the sidescan sonar data. Hence, it is apparent that these seeps have formed in the recent past. However, the lack of acoustic plumes (gas flares) in the water column implies that they are either dormant or expel fluids periodically.

Three distinct acoustic features related to suspected shallow gas occurrences have been recorded in SA1 and SA2 beneath the pockmarked seafloor and inferred seep locations: enhanced reflections, acoustic turbidity and vertical acoustic blankings (Figs. 11, 12). However, it is difficult to quantify the suspected shallow gas in marine sediments based on sub-bottom acoustic data. This is due to the fact that these acoustic features related to assumed gas accumulation and migration may occur due to dissolved or free interstitial gas bubbles ranging from 0.5 to 5 mm in equivalent radius and with 0.5–2% gas by volume (Schubel, 1974; Wilkens & Richardson, 1998).

Unlike other submarine seep sites, where evidence of methane-derived carbonate deposits is usually detected as a high anomaly on multibeam backscatter data (Orange et al., 2002; Judd & Hovland, 2007; Dandapath et al., 2010), we observed low backscatter values from the centre of pockmarks identified on the bathymetric data (Figs. 7C, D, 10). This could suggest possible trapped gas in the shallow, Late Holocene, glacimarine sediments below the pockmarks, which has a low reflectivity as compared to carbonate deposits. The presence of acoustic blankings and turbidity zones beneath these low backscatter locations builds on the interpretation of possible trapped gas beneath pockmarks. The low backscatter strength might also be an outcome of the varying incidence angles at the local depressions of the pockmarks (Fonseca & Mayer, 2007).

Possible source to the seabed seeps and suspected shallow gas

The bedrock in SA2 is largely composed of the Kapp Toscana Group. High-density pockmark zones (>11 pockmarks km^{-2}) have been identified in SA2, east and northeast of ridge R1, which relates to the near top of the Kapp Toscana Group (Figs. 3, 5B, 8). Pockmarks have been found to be aligned along the N–S- to NW–SE-oriented ridges, which are interpreted as seafloor expressions of anticlines linked to the fold-and-thrust belt (Fig. 9) (Roy et al., 2014). The Botneheia Formation forms the bedrock in the eastern part of SA2 (Fig. 2A). Adsorbed and free-gas anomalies in the near-surface marine sediments of inner Isfjorden were shown to reflect a mixture of thermogenic and in situ biologically produced gaseous hydrocarbons (Knies et al., 2004). The thermogenic signature in the bottom marine sediments is found to be dominant along tectonic lineaments. 121 pockmarks are located within 100 m of the sub-cropping faults in SA2 (Fig. 13). The spatial link between pockmarks on the seafloor, underlying shallow gas indicators in marine sediments, the thermogenic signature reported in marine sediments (Knies et al., 2004), and the presence of different types of faults terminating at the seafloor may indicate that fluids were sourced from deeper source rocks. The Middle Triassic Botneheia Formation could be a possible deep thermogenic source rock to the pockmarks and suspected shallow gas found in SA2. The Botneheia Formation has TOC values reaching 12% and is regarded as the main source rock to several petroleum provinces in the southern Barents Sea (Nøttvedt et al., 1993; Bjorøy et al., 2010).

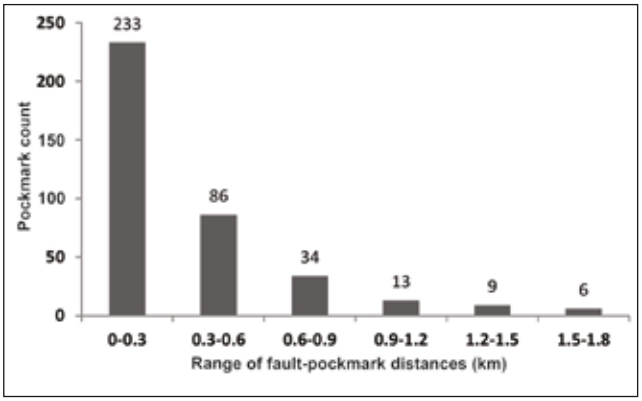

Figure 13. *Histogram plot showing pockmark counts found in each of the fault-pockmark distance ranges in SA2. A near-distance analysis was done on all the pockmarks to calculate their proximity to the mapped faults using the Spatial Analyst tool in ArcGIS software. It shows the relative abundance of pockmarks in close proximity to the faults at different distance ranges.*

The bedrock of SA1 consists predominantly of the Lower Cretaceous Carolinefjellet and Helvetiafjellet formations in the eastern and central parts (Fig. 2A). The Janusfjellet Subgroup comprises part of the fjord bedrock in the northwestern part of SA1, consisting of Upper Jurassic Rurikfjellet and Agardhfjellet formations (Fig. 6B). Traces of hydrocarbons in the Rurikfjellet Formation shale interval have been found in the Longyearbyen CO_2 drillholes Dh4 and Dh5. These wells experienced a gas flux and pressure buildup. The organic-rich shales of the Agardhfjellet Formation have TOC values of 1.5–12% (Dypvik, 1985). East of SA1, hydrocarbon seeps have been documented onshore near to the Jurassic–Cretaceous boundary, with the Agardhfjellet Formation as their most likely source rock (Hammer et al., 2011). We suspect that the organic-rich shales of the Rurikfjellet and Agardhfjellet formations could be potential source rocks to the pockmarks formed in Adventfjorden (SA1). Steeply inclined deep-rooted faults in SA1 (Fig. 7B) suggest that the Middle Triassic Botneheia Formation could also be a possible deeper thermogenic source for seeping fluids (Dypvik, 1985; Nøttvedt et al., 1993; Bjorøy et al., 2010). However, fluids expelled directly from organic-rich bedrock into the soft marine sediments could also be responsible for the formation of pockmarks in SA1 and SA2 (Forwick et al., 2009).

In addition to the thermogenic signature, Knies et al. (2004) have reported a biogenic signature in the marine sediments of inner Isfjorden, which could possibly be gas seeping out from the pockmarks. High sedimentation rates during the deglaciation of the Isfjorden fjord system (Forwick & Vorren, 2010), could have provided anoxic conditions in the fjord-bottom sediments, which is favourable for the production of biogenic gas in the top few metres of the marine glacial and post glacial sediments. Besides thermogenic and biogenic hydrocarbon fluids, pore-water expulsion could not be completely ruled out as a genesis of the pockmarks. The water content in the top 10 m of sediment cores studied from inner Isfjorden is between 15 and 61 wt.% (Forwick & Vorren, 2009). It is likely that due to the suspected shallow gas and sediment diapirism in the marine sediments (Figs. 11, 12), the overpressured pore water migrates upwards utilising minor fractures and permeable pathways, eventually rupturing the seafloor and forming the unit-pockmarks. However, further geochemical analysis of surface sediments and pore fluids can help to explain the source and composition of the fluids seeping from these pockmarks.

Possible migration pathways for fluids

Fold-and-thrust belt complex

Three sheets of thrust faults striking NNW–SSE spread out from the décollement layers with varying frequencies and inclinations in Isfjorden (Bergh et al., 1997; Blinova et al., 2013). Correlation of the bathymetric data and 2D seismic data suggests that the topmost sheet of the fold-and-thrust belt crops out on the seafloor forming ridges (Figs. 5, 8, 9). Thrust faults are composed of fine-grained clay and mud formed due to the shearing between stratigraphic layers (Maher et al., 1986; Braathen & Maher, 1995; Bergh et al., 1997). They have a very low permeability which prohibits free fluid flow. However, upright tight folds and detachment zones represent zones of intense deformation associated with thrust faults, as observed on the seismic dataset (Fig. 5A, B, C). Various types of faults and fracture networks have been documented in the fold-and-thrust belt complex which could provide higher permeability for free fluid flow (Maher et al., 1986; Teyssier et al., 1995; Braathen et al., 2012). According to our interpretations, the thrust faults terminate 50–100 ms (corresponding to 100–220 m depth) beneath the seafloor, but some of the steep faults (yellow lines in Fig. 5A, B, C) and the upright folds (labelled as df) reach the seafloor where pockmarks occur. Fig. 13 shows the proximity analysis of pockmarks from the mapped faults in the shallow stratigraphy, sub-cropping in places on the seafloor in the study area. The occurrence of numerous pockmarks aligned with the ridges interpreted as thrust zones and eroded upright folds suggests a potential for fluid migration along the fractures and steep faults associated with the fold-and-thrust complex (Fig. 9). Shallow and deep faults and the fracture network could provide direct routes for the buoyant hydrocarbon fluids which would then seep through the seafloor forming pockmarks. A dense population of pockmarks has not been found in the southwestern part of the R1 ridge, in contrast to the seafloor located northeast of R1 (Fig. 3). This could be explained by the rare occurrence of steep faults reaching the seafloor, as seen on the seismic profiles, and/or the efficient sealing capacity of the primary cap rock comprising the Janusfjellet Subgroup shales and thus preventing fluid migration from the deeper Middle Triassic source rocks (Braathen et al., 2012).

The southwest-dipping décollement layers are intense zones of shearing, faulting and brecciation. Structural characterisation of core samples from the décollement layer in the Janusfjellet Subgroup documents a high fracture frequency up to 50 f m^{-1} (Braathen et al., 2012). The thrust core consists of strongly crushed and altered shale. Physical property measurements and seismic models of décollement layers in the Nankai Trough and the northern Barbados Ridge have suggested laterally variable fluid pressures migrating from deeper successions along the layer, both up dip and along strike (Hill et al., 1993; Bangs et al., 1996). Based on such fluid-bearing properties of décollement layers, we suggest that the high fracture permeability found within the décollement layer in Isfjorden could permit dewatering of sediments and lateral to upward migration of fluids. Possible fluid migration pathways within the fold-and thrust belt are illustrated in schematic diagrams based on observations made in this study (Fig. 14A).

Deep-rooted faults and associated fractures

The Middle Triassic–Lower Cretaceous succession is characterised by steep faults lying beneath the seafloor of Adventfjorden (Fig. 7B), which displays pockmarks and several unit-pockmarks. A localised fracture-frequency peak associated with a low-angle thrust in the Carolinefjellet Formation (at c. 80 m depth) has been documented in drillholes Dh1 and Dh2 (Braathen et al., 2012). Deep regional faults could provide a direct route for the ascending fluids from potential source rocks (Nøttvedt et al., 1993), which would then apparently leak through the shallow fractures in the bedrock up to the seafloor. However, the length and connectivity of fractures control the fluid conductivity along the fracture network at different stratigraphic depths (Ogata et al., 2012). The presence of sub-seismic faults in the upper part of Kapp Toscana Group as observed in outcrops (Fig. 5D) could also act as fluid conduits in offshore settings.

The migration of fluids within sandstone units is governed by their porosity and permeability. The low permeability (0.01–2 mD) of the Upper Triassic–Middle

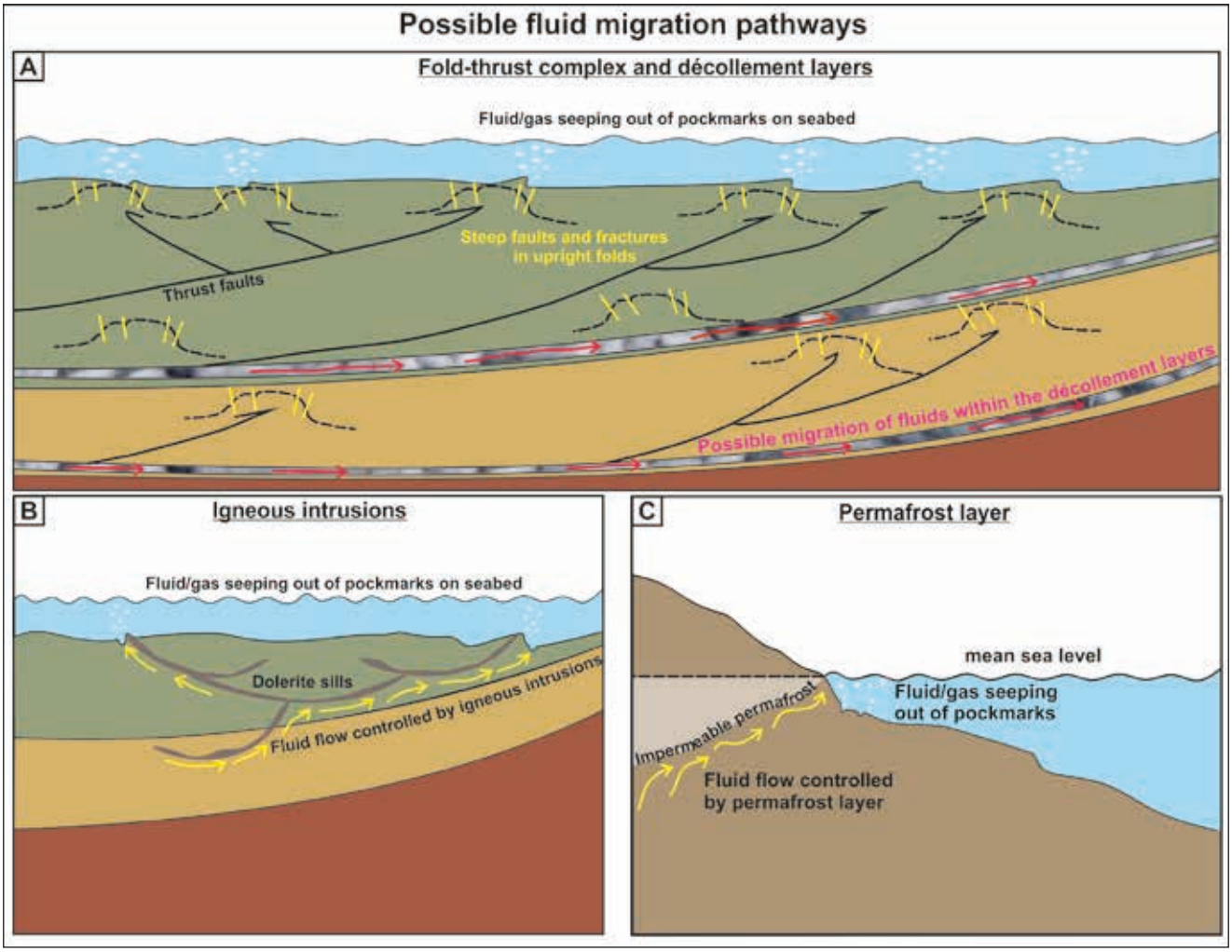

Figure 14. *Conceptual models of natural fluid-migration pathways leading to the formation of pockmarks in Isfjorden, controlled by (A) the fold-thrust complex and décollement layers, (B) Igneous intrusions and (C) the impermeable permafrost layer.*

Jurassic sandstone units, despite their localised moderate to high porosity (2–13% in Dh1 and Dh2, 5–20% in Dh4), is caused by extensive diagenesis associated with compaction, cementation and mineral dissolution (Braathen et al., 2012; Mørk, 2013). Dissolution porosity is the main type of porosity observed in the sandstone units, particularly in the De Geerdalen Formation (Mørk, 2013). However, the low permeability values of the sandstone units would not have allowed a free flow of fluids through them, unless the presence of fractures and faults increased the lateral and vertical connectivity between the pore spaces (Ogata et al., 2014).

Migration and trapping of CO_2 within the aquifer and cap-rock succession

Owing to the dipping regional stratigraphy, it is likely that the injected buoyant CO_2 will migrate upwards and northeastwards where the aquifer unit crops out in onshore and offshore settings. Some of the mobile CO_2 could be physically trapped under the impermeable Janusfjellet Subgroup shales and spread laterally forming a CO_2 plume. Upward-migrating CO_2 could be trapped through residual trapping, chemical dissolution and mineralisation (Pruess, 2008). CO_2 plume movement towards the northeast could be accelerated by decreased overburden pressure and increased permeability in the fractured saline aquifer (Farokhpoor et al., 2011; Ogata et al., 2012, 2014). Sub-vertical fractures are notably common in the targeted aquifer, whereas low-angle fractures dominate near the surface (Braathen et al., 2012). The faster the CO_2 flows through the fracture network, the less time will be available for CO_2 to be trapped as a residual phase and dissolve in the pore water. The un-trapped injected CO_2 will remain in a mobile phase and continue migrating if the integrity of the cap rock is compromised by permeable layers or conduits like well bores, sub-vertical faults and fracture networks. However, in some subsurface environments, CO_2 could be converted to methane mediated by microbes (Hoth et al., 2005). Even if small amounts of CO_2 seep out to the seafloor through the faults and fractures, it is likely to disperse and dissolve in the seawater. Furthermore, water pressure and dilution in oceanic water will prevent direct emission of CO_2 into the air (Pruess, 2008).

The large magnitude of adiabatic cooling resulting from the rising depressurised CO_2 provides a self-limiting feedback to the discharge (Pruess, 2008). The density of the upward-migrating CO_2 increases due to a decline in temperatures. Hence, the buoyancy force pushing the CO_2 upward is also reduced. A good sealing condition is maintained in the aquifer by a considerable under-pressure (equal to 30% of the hydrostatic pressure) in the lower part of the succession (Braathen et al., 2012). Core samples indicate tight reservoir properties within sandstones of moderate porosity (5–18%) and low permeability (max. 1–2 mD) (Braathen et al., 2012; Mørk, 2013). The high capillary pressure can slow down the migration of the CO_2 plume. Simulation results suggest that half of the injected CO_2 would dissolve in the pore water and the other half dispersed within a radius of 1000 m from the wells after 4000 years (Farokhpoor et al., 2010).

Igneous intrusions

Igneous intrusions have been identified in the Kapp Toscana Group as high-amplitude reflections with abrupt terminations on 2D seismic data (Figs. 5A, B, C, 6A). A 2.28 m thick intrusion was penetrated at 950 m by drill hole Dh4 (Senger et al., 2014). A positive strong magnetic anomaly from the resistant ridges mapped on the bathymetric data illustrates their correlation with high-amplitude reflections interpreted as igneous intrusions on 2D seismic profiles (Senger et al., 2013). A high concentration of pockmarks along the outcropping edge of the igneous intrusions has provided circumstantial evidence for focused fluid flow channelling along the base of impermeable dolerite sills to the seafloor northeast of the present study area (Roy et al., 2012; Senger et al., 2013). We therefore suggest that the igneous intrusions identified in the reservoir unit could be crucial in directing the buoyant fluid flow towards the surface (Fig. 14B).

Secondary sealing mechanisms in the Arctic

Permafrost sealing

Harada & Yoshikawa (1998) and Humlum (2005) estimated the Holocene permafrost thickness in the range of 3–100 m in the low-altitude valleys of Longyearbyen. The aquifer and top seal units are sealed with a *c.* 100 m-thick permafrost layer in onshore settings (Humlum, 2005; Braathen et al., 2012). In an attempt to model the extent and possibility of coastal subsea permafrost in western Spitsbergen, Kristensen et al. (2008) suggested that the presence of seawater will affect the ground thermal conditions more than 100 m from the shoreline. The permafrost can act as an additional layer of seal to the injected CO_2 in onshore settings. Owing to the gradual thinning of the permafrost layer towards the coastline, fluids could migrate along the onshore impermeable permafrost and seep through to the seabed where the permafrost is absent (Fig. 14C).

Possible CO_2 hydrate sealing

CO_2 hydrate forms in marine sediments as a result of cold temperatures prevailing in the sea-bottom waters of the High Arctic (Koide et al., 1997; House et al., 2006). Injected CO_2 that migrates upward to cooler temperature conditions in high altitudes saturates the groundwater and can eventually form a CO_2 hydrate cap at a depth of 200 m and 2°C (Teng et al., 1996). Sea-bottom water temperatures range from -2 to 5°C in the whole of Isfjorden at water depths greater than 250 m, providing stable conditions for the formation of a hydrate layer of CO_2 droplets on the surface in high-pressure and low-temperature conditions (Teng et al., 1996; Roy et al., 2012). Possible CO_2 hydrate formation in the submarine sediment pores and beneath the onshore permafrost can impede the flow of CO_2 and serve as a secondary seal on the aquifer.

Conclusions

Based on the integrated analysis of the high-resolution geophysical datasets along with the structural mapping of the fold-thrust belt complex in the aquifer and cap-rock succession, we conclude the following:

- 398 pockmarks mapped on the multibeam bathymetric data provide evidence of past seepage of natural fluids to the seafloor.
- The occurrence of unit-pockmark clusters suggests a possible ongoing seepage of fluids. The combined presence of turbidity zones and enhanced reflectors in the marine sediments beneath the densely pockmarked seafloor suggests the presence of suspected gas in the shallow stratigraphy of the two study areas.
- Vertical acoustic blankings (gas chimneys) detected in shallow sediments and low backscatter anomalies from pockmarks suggest possible gas migration through marine sediments and the presence of trapped gas within the surface sediments of the pockmarks, respectively.
- The spatial linkage and alignment of pockmarks with the ridges, which are interpreted as seafloor expressions of the fold-and-thrust complex, suggest a focused fluid migration along thrust faults in inner Isfjorden.
- The presence of deep faults in the reservoir and cap-rock succession possibly plays a vital role in the vertical ascent of fluids and hence generation of pockmarks in Adventfjorden.
- The evidence of focused fluid seeps on the seafloor, suspected shallow gas occurrences located above shallow- and deep-rooted sub-horizontal to vertical faults spreading from the décollement layers and fractured bedrock affected by the fold-and-thrust belt suggests that fluids possibly follow(ed): sub-horizontal to vertical permeable pathways.
- The mapped thrust faults sub-cropping on the seafloor and seep locations identified on bathymetric and sidescan sonar data could be potential sites for future monitoring of possible CO_2 migration.

Geochemical analyses of the pore fluids are needed for linking the seabed seeps to potential sources and for a better understanding of their migration processes.

Acknowledgements. This study is part of the *High North Research Project* investigating the *Barents Sea source rocks*, funded by ConocoPhillips, Lundin Petroleum AS and the UNIS CO_2 lab project in Longyearbyen (http://co2-ccs.unis.no). We acknowledge the Norwegian Hydrographic Service for providing access to the high-resolution multibeam bathymetric data (permission number: 13/G706). We are grateful to Statoil and participants of the Svalex expeditions, Prof. Rolf Mjelde of University of Bergen for generously providing access to the multichannel 2D seismic data. Schlumberger provided an academic license of Petrel. We thank the crews of R/V Jan Mayen (now Helmer Hanssen) and Viking Explorer for their support in the geophysical data acquisition. We are also thankful to the Research Council of Norway for the research grant to Srikumar Roy. Finally, special thanks to the reviewer Reidulv Bøe and the editor Trond Slagstad, for their insightful comments on the manuscript.

References

Bachu, S. 2008: CO_2 storage in geological media: Role, means, status and barriers to deployment. *Progress in Energy and Combustion Science 34*, 254–273.

Bangs, N.L., Shipley, T.H. & Moore, G.F. 1996: Elevated fluid pressure and fault zone dilation inferred from seismic models of the northern Barbados Ridge décollement. *Journal of Geophysical Research: Solid Earth 101*, 627–642.

Bergh, S.G., Braathen, A. & Andresen, A. 1997: Interaction of basement-involved and thin-skinned tectonism in the Tertiary fold-thrust belt of central Spitsbergen, Svalbard. *American Association of Petroleum Geologists Bulletin 81*, 637–661.

Bjorøy, M., Hall, P.B., Ferriday, I.L. & Mørk, A. 2010: Triassic Source Rocks of the Barents Sea and Svalbard. *Abstracts and Proceedings, American Association of Petroleum Geologists Convention*, 7–10 June, Denver, Colorado, USA, Article No. 10219, 8 pp.

Blinova, M., Faleide, J.I., Gabrielsen, R.H. & Mjelde, R. 2012: Seafloor expression and shallow structure of a fold-and-thrust system: Isfjorden, West Spitsbergen. *Polar Research 31*, 11209, http://dx.doi.org/10.3402/polar.v31i0.11209.

Blinova, M., Faleide, J.I., Gabrielsen, R.H. & Mjelde, R. 2013: Analysis of structural trends of sub-sea-floor strata in the Isfjorden area of the West Spitsbergen Fold-and-Thrust Belt based on multichannel seismic data. *Journal of the Geological Society of London 170*, 657–668.

Boyer, S.E. & Elliott, D. 1982: Thrust systems. *American Association of Petroleum Geologists Bulletin 66*, 1196–1230.

Braathen, A. & Bergh, S.G. 1995: Kinematics of Tertiary deformation in the basement-involved fold-thrust complex, western Nordenskiøld Land, Svalbard: tectonic implications based on fault-slip data analysis. *Tectonophysics 249*, 1–29.

Braathen, A. & Maher, H.D. 1995: Structural outline of a Tertiary Basement-cored uplift/inversion structure in western Spitsbergen, Svalbard: Kinematics and controlling factors. *Tectonics 14*, 95–119.

Braathen, A., Bergh, S.G. & Maher, H.D. 1999: Application of a critical wedge taper model to the Tertiary transpressional fold-thrust belt on Spitsbergen, Svalbard. *Geological Society of America Bulletin 111*, 1468–1485.

Braathen, A., Bælum, K., Christiansen, H.H., Dahl, T., Eiken, O., Elvebakk, H., Hansen, F., Hanssen, T.H., Jochmann, M., Johansen, T.A., Johnsen, H., Larsen, L., Lie, T., Mertes, J., Mørk, A., Mørk, M.B., Nemec, W., Olaussen, S., Oye, V., Rød, K., Titlestad, G.O., Tveranger, J. & Vagle, K. 2012: The Longyearbyen CO_2 Lab of Svalbard, Norway— initial assessment of the geological conditions for CO_2 sequestration. *Norwegian Journal of Geology 92*, 353–376.

Bælum, K., Johansen, T.A., Johnsen, H., Rød, K., Ruud, B.O. & Braathen, A. 2012: Subsurface structures of the Longyearbyen CO_2 Lab study area in Central Spitsbergen (Arctic Norway), as mapped by reflection seismic data. *Norwegian Journal of Geology 92*, 377–389.

Bælum, K. & Braathen, A. 2012. Along-strike changes in fault array and rift basin geometry of the Carboniferous Billefjorden Trough, Svalbard, Norway. *Tectonophysics 546–547*, 38–55.

Chadwick, R.A., Arts, R., Bentham, M., Eiken, O., Holloway, S., Kirby, G.A., Pearce, J.M., Williamson, J.P. & Zweigel, P. 2009: Review of monitoring issues and technologies associated with the long-term underground storage of carbon dioxide. *Journal of the Geological Society of London, Special Publications 313*, 257–275.

Collier, J.S. & Brown, C.J. 2005: Correlation of sidescan backscatter with grain size distribution of surficial seabed sediments. *Marine Geology 214*, 431–449.

Corfu, F., Polteau, S., Planke, S., Faleide, J.I., Svensen, H., Zayoncheck, A. & Stolbov, N. 2013: U–Pb geochronology of Cretaceous magmatism on Svalbard and Franz Josef Land, Barents Sea Large Igneous Province. *Geological Magazine 150*, 1127–1135.

Dallmann, W.K., Ohta, Y., Elvevold, S. & Blomeier, D. 2002: Bedrock map of Svalbard and Jan Mayen. *Norsk Polarinstitutt Temakart 33*.

Damm, E., Mackensen, A., Budéus, G., Faber, E. & Hanfland, C. 2005: Pathways of methane in seawater: Plume spreading in an Arctic shelf environment (SW-Spitsbergen). *Continental Shelf Research 25*, 1453–1472.

Dandapath, S., Chakraborty, B., Karisiddaiah, S.M., Menezes, A., Ranade, G., Fernandes, W., Naik, D.K. & Prudhvi Raju, K.N. 2010: Morphology of pockmarks along the western continental margin of India: Employing multibeam bathymetry and backscatter data. *Journal of Marine and Petroleum Geology 27*, 2107–2117.

Digranes, P. & Kristoffersen, Y. 1995: Use of mode-converted waves in marine seismic data to investigate the lithology of the sub-bottom sediments in Isfjorden, Svalbard. *Journal Pure and Applied Geophysics 145*, 313–325.

Dypvik, H. 1985: Jurassic and Cretaceous black shales of the Janusfjellet Formation, Svalbard, Norway. *Sedimentary Geology 41*, 235–248.

Farokhpoor, R., Torsæter, O., Baghbanbashi, T., Mørk, A. & Lindeberg, E.G.B. 2010: Experimental and Numerical Simulation of CO_2 Injection into Upper-Triassic Sandstones in Svalbard, Norway. *Abstracts and Proceedings, Society of Petroleum Engineers International Conference on CO_2 Capture, Storage, and Utilization, 10–12 November, New Orleans, Louisiana, USA*, SPE 139524.

Farokhpoor, R., Baghbanbashi, T., Torsæter, O., Lindeberg, E. & Mørk, A. 2011: Experimental and Simulation Analysis of CO_2 Storage in Tight and Fractured Sandstone under Different Stress Conditions. *Abstracts and Proceedings, Society of Petroleum Engineers Annual Conference and Exhibition, 23–26 May, Vienna, Austria*, SPE 143589.

Fonseca, L. & Mayer, L. 2007: Remote estimation of surficial seafloor properties through the application Angular Range Analysis to multibeam sonar data. *Marine Geophysical Researches 28*, 119–126.

Forwick, M. & Vorren, T.O. 2009: Late Weichselian and Holocene sedimentary environments and ice rafting in Isfjorden, Spitsbergen. *Palaeogeography, Palaeoclimatology, Palaeoecology 280*, 258–274.

Forwick, M. & Vorren, T.O. 2010: Stratigraphy and deglaciation of the Isfjorden area, Spitsbergen. *Norwegian Journal of Geology 90*, 163–179.

Forwick, M., Baeten, N.J. & Vorren, T.O. 2009: Pockmarks in Spitsbergen fjords. *Norwegian Journal of Geology 89*, 65–77.

Gaina, C., Gernigon, L. & Ball, P. 2009: Palaeocene–Recent plate boundaries in the NE Atlantic and the formation of the Jan Mayen microcontinent. *Journal of the Geological Society of London 166*, 601–616.

Hammer, O., Nakrem, H.A., Little, C.T.S., Hryniewicz, K., Sandy, M.R., Hurum, J.H., Druckenmiller, P., Knutsen, E.M. & Høyberget, M. 2011: Hydrocarbon seeps from close to the Jurassic–Cretaceous boundary, Svalbard. *Palaeogeography, Palaeoclimatology, Palaeoecology 306*, 15–26.

Hansen, D.M., Cartwright, J.A. & Thomas, D. 2004: 3D Seismic Analysis of the Geometry of Igneous Sills and Sill Junction Relationships. *Geological Society of London, Memoirs 29*, 199–208.

Harada, K. & Yoshikawa, K. 1998: Permafrost Age and thickness at Moskuslagoon, Spitsbergen. *Abstracts and Proceedings, Seventh International Conference on Permafrost. Yellowknife, Canada, Collection Nordicana No 55*, pp. 427–431.

Harland, W.B. 1997: The Geology of Svalbard, *Geological Society, London*, 521 pp.

Henriksen, E., Ryseth, A.E., Larssen, G.B., Heide, T., Rønning, K., Sollid, K. & Stoupakova, A.V. 2011: Chapter 10 Tectonostratigraphy of the greater Barents Sea: implications for petroleum systems. *Geological Society of London, Memoirs 35,* 163–195.

Hill, L., Taira, A. & Firth, J.V. 1993: Character of the décollement in the Leg 131 area, Nankai Trough. *Proceedings of the Ocean Drilling Program, Scientific Results*, p. 131.

Hosa, A., Esentia, M., Stewart, J. & Haszeldine, S. 2011: Injection of CO_2 into saline formations: Benchmarking worldwide projects. *Chemical Engineering Research and Design 89*, 1855–1864.

Hoth, N., Schlömann, M., Kassahun, A., Glombitza, F. & Häfner, F. 2005: Recycling of sequestered CO_2 by microbial-biogeochemical transformation in the deep subsurface (RECOBIO). *In* Stroink, L. (ed.): *Investigation, Utilization and protection of the underground*, Geotechnologien Science Report No. 6, Geoforschungszentrum, Potsdam, Germany, pp. 14–27.

House, K.Z., Schrag, D.P., Harvey, C.F. & Lackner, K.S. 2006: Permanent carbon dioxide storage in deep-sea sediments. *Proceedings of the National Academy of Sciences 103*, 12291–12295.

Hovland, M. & Judd, A.G. 1988: Seabed pockmarks and seepages: *Impact on Geology, Biology and the Marine Environment.* Graham & Trotman Ltd., London, 193 pp.

Hovland, M. & Curzi, P.V. 1989: Gas seepage and assumed mud diapirism in the Italian central Adriatic Sea. *Journal of Marine and Petroleum Geology 6*, 161–169.

Hovland, M., Heggland, R., Vries, M.H.D. & Tjelta, T.I. 2010: Unit-pockmarks and their potential significance for predicting fluid flow. *Journal of Marine and Petroleum Geology 27*, 1190–1199.

Humlum, O. 2005: Holocene permafrost aggradation in Svalbard. *Geological Society of London, Special Publications 242*, 119–129.

Jenkins, C.R., Cook, P.J., Ennis-King, J., Undershultz, J., Boreham, C., Dance, T., de Caritat, P., Etheridge, D.M., Freifeld, B.M., Hortle, A., Kirste, D., Paterson, L., Pevzner, R., Schacht, U., Sharma, S., Stalker, L. & Urosevic, M. 2012: Safe storage and effective monitoring of CO_2 in depleted gas fields. *Proceedings of the National Academy of Sciences 109*, E35–E41.

Judd, A.G. & Hovland, M. 1992: The evidence of shallow gas in marine sediments. *Continental Shelf Research 12*, 1081–1095.

Judd, A.G. & Hovland, M. 2007: *Seabed Fluid Flow, the Impact on Geology, Biology, and the Marine Environmentk.* Cambridge University Press, Cambridge, 475 pp.

Knies, J., Damm, E., Julian Gutt, U.M. & Pinturier, L. 2004: Near-surface hydrocarbon anomalies in shelf sediments off Spitsbergen: Evidences for past seepages. *Geochemistry Geophysics Geosystems G3 5*, 1–14.

Koide, H., Takahashi, M., Shindo, Y., Tazaki, Y., Iijima, M., Ito, K., Kimura, N. & Omata, K. 1997: Hydrate formation in sediments in the sub-seabed disposal of CO_2. *Energy 22*, 279–283.

Kristensen, L., Christiansen, H.H. & Caline, F. 2008: Temperatures in Coastal Permafrost in the Svea Area, Svalbard. *Abstracts and Proceedings, Ninth International Conference on Permafrost, 29 June – 3 July, Fairbanks, Alaska, USA*, p. 1005-1010.

Larssen, G., Bjørnseth, H., Kløvjan, O., Kåsli, K., Ryseth, A., Rønning, K., Stoupakova, A., Laursen, I. & Sollid, K. 2012: The Barents Sea-Back in Business, *Abstracts and Proceedings, 74th European Association of Geoscientists and Engineers Conference & Exhibition, 4–7 June, Copenhagen, Denmark.*

Leever, K.A., Gabrielsen, R.H., Faleide, J.I. & Braathen, A. 2011: A transpressional origin for the West Spitsbergen fold-and-thrust belt: Insight from analog modeling. *Tectonics 30*, doi: 10.1029/2010TC002753.

Lewicki, J., Birkholzer, J. & Tsang, C.-F. 2007: Natural and industrial analogues for leakage of CO_2 from storage reservoirs: identification of features, events, and processes and lessons learned. *Environmental Geology 52*, 457–467.

Maher, H.D., Craddock, C. & Maher, K. 1986: Kinematics of Tertiary structures in upper Paleozoic and Mesozoic strata on Midterhuken, west Spitsbergen. *Geological Society of America Bulletin 97*, 1411–1421.

McQuillin, R., Bacon, M. & Barclay, W. 1984: *An introduction to seismic interpretation - Reflection seismics in petroleum exploration*. Graham & Trotman, London, 287 pp.

Mørk, M.B.E. 2013: Diagenesis and quartz cement distribution of low-permeability Upper Triassic–Middle Jurassic reservoir sandstones, Longyearbyen CO_2 lab well site in Svalbard, Norway. *American Association of Petroleum Geologists Bulletin 97*, 577–596.

Nøttvedt, A., Livbjerg, F., Midbøe, P.S. & Rasmussen, E. 1993: Hydrocarbon potential of the Central Spitsbergen Basin. *In* Vorren, T.O., Bergsager, E., Dahl -Stamnes, Ø.A., Holter, E., Johansen, B., Lie, E. & Lund, T.B. (eds.): *Arctic Geology and Petroleum Potential*, Norwegian Petroleum Society Special publication no. 2, Amsterdam, Elsevier, pp. 333–361.

Ogata, K., Senger, K., Braathen, A., Tveranger, J. & Olaussen, S. 2012: The importance of natural fractures in a tight reservoir for potential CO_2 storage: a case study of the upper Triassic–middle Jurassic Kapp Toscana Group (Spitsbergen, Arctic Norway). *In* Spence, G.H., Redfern, J., Aguilera, R., Bevan, T.G., Cosgrove, J.W., Couples, G.D. & Daniel, J.-M. (eds.): *Advances in the Study of Fractured Reservoirs*, Geological Society of London Special Publication 371, PAGES, doi: 10.1144/sp374.9.

Ogata, K., Senger, K., Braathen, A., Tveranger, J. & Olaussen, S. (2014): Fracture systems and meso-scale structural patterns in the siliciclastic Mesozoic reservoir-caprock succession of the Longyearbyen CO_2 Lab project: implications for geologic CO_2 sequestration on Central Spitsbergen, Svalbard. *Norwegian Journal of Geology 94*, 121-154.

Orange, D.L., Yun, J., Maher, N., Barry, J. & Greene, G. 2002: Tracking California seafloor seeps with bathymetry, backscatter and ROVs. *Continental Shelf Research 22*, 2273–2290.

Pruess, K. 2008: On CO_2 fluid flow and heat transfer behavior in the subsurface, following leakage from a geologic storage reservoir. *Environmental Geology 54*, 1677–1686.

Ross, N., Harris, C., Christiansen, H.H. & Brabham, P.J. 2005: Ground penetrating radar investigations of open system pingos, Adventdalen, Svalbard. *Norsk Geografisk Tidsskrift - Norwegian Journal of Geography 59*, 129–138.

Roy, S., Senger, K., Noormets, R. & Hovland, M. 2012: Pockmarks in the fjords of western Svalbard and their implications on gas hydrate dissociation. *Geophysical Research Abstracts 14*, p. 8960.

Roy, S., Noormets, R. & Braathen, A. 2014: Seafloor expressions of tectonic structures in Isfjorden, Svalbard: implications for fluid migration. *Geophysical Research Abstracts 16*, p. 9774.

Schroot, B.M., Klaver, G.T. & Schüttenhelm, R.T.E. 2005: Surface and subsurface expressions of gas seepage to the seabed—examples from the Southern North Sea. *Journal of Marine and Petroleum Geology 22*, 499–515.

Schubel, J.R. 1974: Gas Bubbles and the Acoustically Impenetrable, or Turbid, Character of Some Estuarine Sediments. *In* Kaplan, I. (ed.): *Natural Gases in Marine Sediments.* Springer, New York, pp. 275–298.

Senger, K., Roy, S., Braathen, A., Buckley, S., Bælum, K., Gernigon, L., Mjelde, R., Noormets, R., Ogata, K., Olaussen, S., Planke, S., Ruud, B. & Tveranger, J. 2013: Geometries of doleritic intrusions in central Spitsbergen, Svalbard: an integrated study of an onshore-offshore magmatic province with implications for CO_2 sequestration. *Norwegian Journal of Geology 93*, 143–166.

Senger, K., Svensen, H., Planke, S. & Polteau, S. (2014): Dolerite intrusions within the Kapp Toscana Group in Central Spitsbergen, Svalbard: contact metamorphism and impact on reservoir properties. *Norwegian Journal of Geology 94*, 155–169.

Steel, R. & Worsley, D. 1984: Svalbard's post-Caledonian strata — an atlas of sedimentational patterns and palaeogeographic evolution. *In* Spencer, A.M. (ed.): *Petroleum Geology of the North European Margin*. Springer Netherlands, London, pp. 109–135.

Steel, R.J., Dalland, A., Kalgraff, K. & Larsen, V. 1981: The Central Tertiary Basin of Spitsbergen: Sedimentary Development of a Sheared-Margin Basin. *Canadian Society of Petroleum Geologists Special Publications 7*, 647–664.

Talwani, M. & Eldholm, O. 1977: Evolution of the Norwegian-Greenland Sea. Geological Society of America Bulletin 88, 969–999.

Teng, H., Yamasaki, A. & Shindo, Y. 1996: Stability of the hydrate layer formed on the surface of a CO_2 droplet in high-pressure, low-temperature water. *Chemical Engineering Science 51*, 4979–4986.

Teyssier, C., Kleinspehn, K. & Pershing, J. 1995: Analysis of fault populations in western Spitsbergen: Implications for deformation partitioning along transform margins. *Geological Society of America Bulletin 107*, 68–82.

Wilkens, R.H. & Richardson, M.D. 1998: The influence of gas bubbles on sediment acoustic properties: in situ, laboratory, and theoretical results from Eckernförde Bay, Baltic sea. *Continental Shelf Research 18*, 1859–1892.

Woodward, N.B. & Rutherford Jr., E. 1989: Structural lithic units in external orogenic zones. *Tectonophysics 158*, 247–267.

Worsley, D. 2008: The post-Caledonian development of Svalbard and the western Barents Sea. *Polar Research 27*, 298–317.

Yoshikawa, K. & Harada, K. 1995: Observations on Nearshore Pingo Growth, Adventladen, Spitsbergen. *Permafrost And Periglacial Processes 6*, 361–372.